UiT
THE ARCTIC
UNIVERSITY
OF NORWAY

Faculty of Science and Technology
Department of Physics and Technology

A Comparison of Naturally Enhanced Ion Acoustic Lines and Auroral Spectral Line Emissions

Rikke Hedelund Hansen

FYS-3931 Master Thesis in Space Physics, June 2019

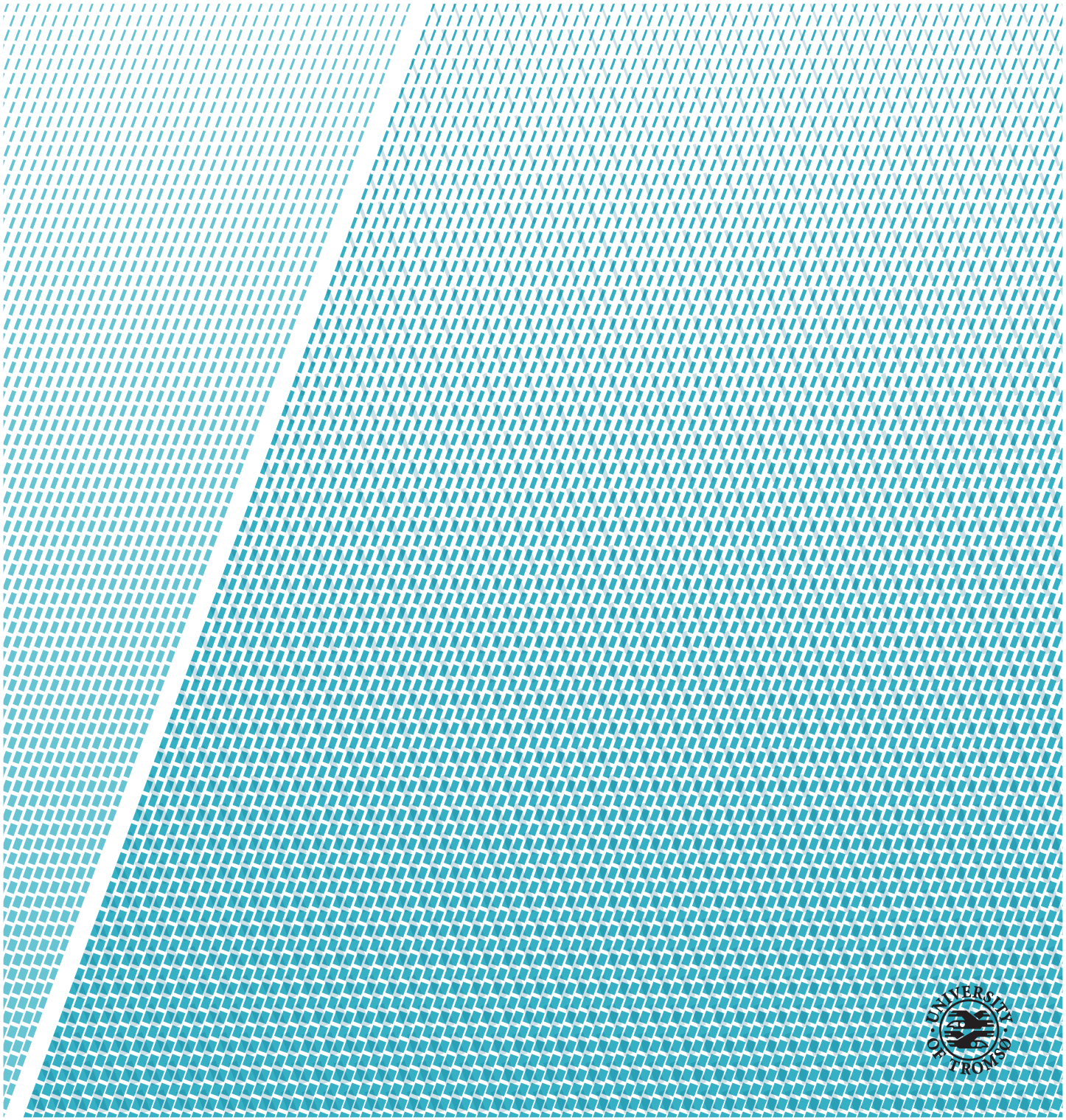

Abstract

In this thesis, we present Naturally Enhanced Ion Acoustic Lines (NEIALs) observed with the EISCAT Svalbard Radar and a comparison with auroral emissions lines measured with a Meridian Scanning Photometer. NEIALs are short-lived events noticeable in the incoherent scatter spectra as an enhancement in one or both shoulders.

It has been assumed that NEIALs are associated with an active red emission line in the aurora with an intensity above 10 kR. The red emission line intensity is associated with soft particle precipitation. However, NEIALs have also been observed at low altitudes where particles with higher energies are present, and they are also associated with a severe geomagnetic activity (>500 nT).

In the literature, there are three competing theories which might explain the cause of NEIALs in the ionosphere, and they all require free energy provided by auroral particle precipitation. The theories are associated with partly different energy ranges, and auroral emission lines may give an indication of the energies of the precipitating particles.

We analyzed four separate days where there were NEIAL incidents. For most of the events, the red line intensity was greater than 10 kR. This agrees with previous observations, and it supports the parametric decay of Langmuir wave theory, which requires soft particles precipitation. However, we have identified 7 events where the red line intensities were below 10 kR, and this weakens the requirement of 10 kR for NEIALs to appear.

When NEIALs were observed at lower altitudes (<400 km), the intensity of the green line increased and the right shoulder in the spectra was the most enhanced. This could suggest that at these altitudes, the current driven instability might be the prevailing theory for the production of NEIALs.

We also found that increased power in the incoherent scatter spectra might be associated with enhancements in the red line intensity. NEIALs were also observed when the geomagnetic activity was below 500 nT.

Acknowledgements

I want to thank my superb advisor Unni Pia Løvhaug for all the help and for introducing me to this fun task. Thank you for just always being open for discussions. I want to thank Bjørn Guvstavsson for all the help with the programming and for just being there when he was needed.

I also want to thank Magnar Gullikstad Johnsen for helping me with the magnetometer and the different indices. I want to thank Lindis for proofreading the thesis, providing me the data, and by helping me when needed. She was just an email away.

I want to thank all the master students in the space physics group. It was fun with the discussions, and the social stuff we did together.

I want to thank my family for proofreading and calming me when I was stressed. And always supporting me.

Finally, I want to thank Tromsø. It was an fantastic adventure, and you will always be in my heart.

Contents

List of Figures

List of Tables

1 Introduction

A Naturally Enhanced Ion Acoustic Line (NEIAL) is a phenomenon in the ionosphere. It is an enhancement in one or both shoulders of the power spectra from an incoherent scatter radar. The first to detect the phenomenon was Foster et al. [1988] with the Millstone Hill located in Westford in Massachusetts, USA. The Millstone Hill radar was pointing towards north parallel to the magnetic field and an asymmetric incoherent scatter spectrum was observed.

The first to observe this phenomenon at higher latitudes and within the auroral oval was Rietveld et al. [1991]. They observed a severe geomagnetic activity along with NEAILs. Collis et al. [1991] observed NEIALs with a red aurora intensity above 10 kR. They argued that these observations and soft particle precipitation had to be associated with NEIALs.

Lunde et al. [2007, 2009] investigated NEIALs with data from the Meridian Scanning Photometer instrument to see which emission lines were active, their intensities and the energy related to the intensity. They state that the 844.6 nm line is a better indicator of NEIALs than the red line intensity.

Several observations of NEIALs have been reported in the literature since 1991 (Sedgemore-Schulthess and Maurice [2001] and reference therein), and three theories have emerged to be able to explain the NEIALs phenomena. The first theory about NEIALs was that these events occurred because of high local currents [Rietveld et al., 1991]. Such high currents were not measured at that time and therefore, this theory was rejected in the 90*s*. The second theory

was about ion-ion two-stream instabilities proposed by Wahlund et al. [1992]. This theory had problems explaining the enhancements in both shoulders in the incoherent scatter spectrum. The theory requires a relative drift between the ions which would only be possible at very high altitudes. In the late 90s and beginning of the 2000, Forme [1993] introduced the theory parametric decay of Langmuir waves where the NEAILs were caused by a bump in the tail in the electron velocity distribution. This theory is associated with electron precipitation of 500 eV and the associated red line intensity. Therefore, the theory may have problems explaining NEIALs that have been observed down to 120 km altitude where the red line is less active.

The parametric decay of Langmuir waves is the prevailing theory and has been supported by the simultaneous observations of plasma lines [Strømme et al., 2005]. Also, the lack of measurements of the intense currents in the ionosphere required for the current driven instability has been an argument for the parametric decay of Langmuir waves theory to be the main theory. However, in 2003, high local current densities in the ionosphere were detected by the Ørsted satellite [Neubert and Christiansen, 2003].

All three theories mentioned above have been modeled and found to explain the enhancement in the shoulders in the incoherent scatter spectrum. In this thesis, we compare the NEIALs characteristics with data from the Meridian Scanning Photometer instrument in order to get information about the intensities of the different emission lines. This information will help to asses the amount of energy required for the NEIALs and how they are connected to the theories.

In chapter 2 we present a description of the ionosphere, the aurora and emission lines, the incoherent scatter spectrum, NEIALs and their theories. The instruments are described in chapter 3

We used GUISDAP (Grand Unified Incoherent Scatter Design and Analysis Package) and created functions to find and present the enhancements of the ion lines, and made intensities plots for the field-aligned position from the Meridian Scanning Photometer data — the observations and results of the experiments are found in chapter 4.

Chapter 5 and 6 contains discussions about our results and a conclusion, respectively.

2 Background

2.1 The Ionosphere

The ionosphere is defined as the part of the Earth's atmosphere where the particles are partly ionized. The first to suggest the existence of the ionosphere was Carl Gauss, who had a theory that electric currents in the atmosphere were the reason for variations of the magnetic field e.g.[Schunk and Nagy, 2009].

The ionosphere was discovered by an experiment by Marconi in 1901, where radio waves were reflected and it was assumed there was a conductive electric layer. In 1902, Kennelly and Heaviside explained the experiment with the reflection of waves due to free electron charges e.g [Schunk and Nagy, 2009]. It was later discovered that the high concentration of free electrons was the reason.

The ionosphere starts at approximately 60 km and ends around 1000 km, see e.g [Schunk and Nagy, 2009]. The ionosphere is mainly created by the interaction between ionizing solar ultraviolet radiation (UV) and the Earth's atmosphere by photoionization. Photoionization is a process where solar photons interact with atoms or molecules to ionize the atmosphere. The photoionization is the primary source of the plasma production in the ionosphere e.g [Brekke, 2012]. Several other processes which affect the plasma densities in the ionosphere occur, like recombination of ions with electrons, transport or diffusion of ions and chemical reactions between ions and neutrals [Schunk and Nagy,

2009].

The reflection of a radio wave is dependent on the critical frequency in the ionosphere. This frequency is the highest frequency to be reflected from the ionosphere, and it happens when the radio frequency is equal to the plasma frequency. It is given by

$$f_c = 9 \cdot \sqrt{N} \tag{2.1}$$

where N is the number of electrons per m^3. As long as the frequency is above the critical frequency, the wave can penetrate the ionosphere. The radar frequency of an incoherent scatter radar must be higher than the critical frequency. Equation 2.1 is dependent on the electron density which varies with altitude. The variation of the electron density has a type of structure as shown in Figure 2.1.

This structure of the electron density is divided into layers. These layers are dependent on the photoionization which is dependent on the Sun's activity. The structure has different layers during day and night time. At night time, there are usually two layers; E layer and F layer. At day time, there are three layers: D layer, E layer, F layer, shown in Figure 2.1.

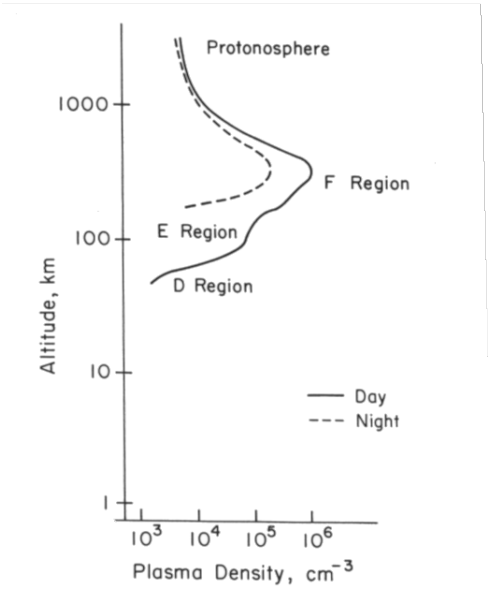

Figure 2.1: The electron density shown with the layers. The dotted line is for night and solid line for day conditions. Based on Kelley [1989].

The D layer covers the altitude range from 60 km to 90 km. The main reason

for the ionization of this layer is the Lyman α series with a wavelength of 121.6 nm. It can also be ionized by X-ray and UV radiation if the solar activity is high. The D layer is very weakly ionized, and neutral gas dynamics dominate. The most dominant species are N_2, O_2 and O and the chemistry is complicated here [Brekke, 2012].

The E layer is from 90 km to 150 km. The X-ray and UV radiation from the sun is the main source of ionization. The electron density is reduced at night. N_2^+ and O_2^+ are the dominating species in this layer [Chernyshov, 2019].

The F layer is from 150 km to approximately 1000 km. Extreme UV radiation produces this layer. The F layer is dominated by atomic species and therefore has a lower recombination rate causing a high electron density. The dominating species is atomic oxygen ions [Brekke, 2012, Chernyshov, 2019].

Above the F layer, the ionosphere decreases with altitude and the ions are dominated by O^+, helium ions and protons [Rishbeth and Garriott, 1969].

2.2 Aurora Borealis

2.2.1 General

Aurora Borealis, also called the northern lights, is a phenomenon in the North where we can see visible colors on a cloudless sky.

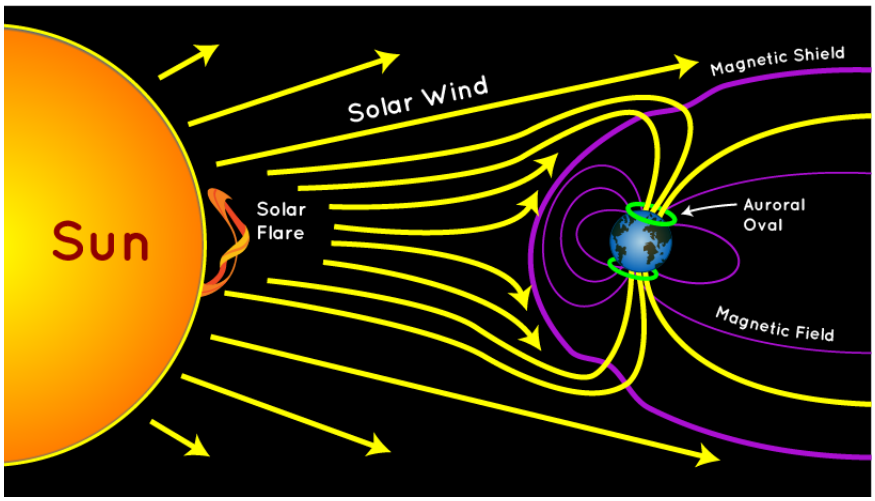

Figure 2.2: A graphic view of the process to create aurora borealis. Credit: NOAA/JPL-Caltech.

In Figure 2.2, there is a graphic picture of the process which creates the aurora. The descriptions of the process of the aurora is explained below.

The aurora is dependent on the activity of the Sun. This activity follows an 11-year cycle depending on the so-called sunspot numbers, and it will increase and decrease along the cycle [Brekke, 2012]. When solar activity is high, the solar wind will be stronger.
The solar wind is a continuous flow of plasma from the Sun. Sometimes there is a Coronal Mass Ejection (CME) from solar flares which are associated with the sunspots that make the solar wind [Prölss, 2004]. In these areas, the particles, such as electrons and protons, can escape the gravity of the Sun. These CMEs increase the solar wind velocities and densities. The solar wind is "frozen-in" into the magnetic field of the Sun, the Interplanetary Magnetic Field (IMF), and the densities of the particles will decrease with distance from the Sun.

The solar wind will hit the Earth's magnetic field and compress the magnetic field lines on the dayside. The particles will deflect, and most of them will travel outside the magnetopause and continue to the nightside. In the magnetospheric tail, the particles enter the magnetic field and are accelerated back towards the Earth along the field lines. Closer to the Earth, the particles are guided to the north and the south auroral ovals. These particles will collide with the particles in the Earth's atmosphere and cause ionization or excite the particle.

The excited particles will have a higher unstable energy level. Some of the particles will emit light after the particles lifetime. This is because the energy level is unstable and will go back to the stable energy level after the particle lifetime of the excited state.
Because of the position of the auroral oval depends on the geomagnetic activity and the Sun's activity, the size of the oval will vary depending on geomagnetic conditions. So for a quiet magnetic disturbed day, the auroral oval will not include the latitude of Svalbard at nightside, but will be included at the dayside.

2.2.2 Dayside aurora

Dayside northern lights are different from those on the nightside. the energetic particles can penetrate directly into the atmosphere because the polar cusp magnetic field lines are open to the interplanetary space. The energy of the incoming particles are typical below 1 keV. The red emission line, 630.0 nm, will dominate the daytime aurora where atomic oxygen is abundant. Soft fluxes of magneto-sheath particle precipitation are the cause of the 630.0 nm emissions [Carlson Jr. and Egeland, 1995].

The auroral emissions are described in terms of spectral emissions. They are dependent on the type of particle and the energy level of the excited state.

2.2.3 Spectral Emissions

A photon can excite and potentially ionize an atom or a molecule.

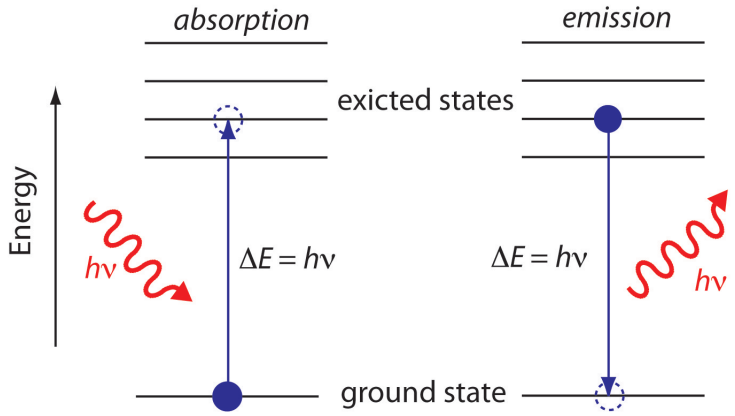

Figure 2.3: Graphic design of the process of the excitation of a particle and the emission. Courtesy Harvey [2013].

Figure 2.3 shows a graphic design of how the excitation and emission may happen. The Figure shows a general case, and does not represent a specific particle. The blue circle represents the particle which is excited after being hit by an electron. When the particle returns to the ground state, a photon is emitted with energy $h\nu$.
The electron impact equation (equation 2.2) shows the result of the particle collisions. Equation 2.3 shows the Cascading equation which indicates the result after a particle excitation. [Carlson Jr. and Egeland, 1995].

$$e + N \longrightarrow N^{*} + e^{'} \tag{2.2}$$

$$N^{**} \longrightarrow N^{*} + h\nu \tag{2.3}$$

In these equations, N is an atom or a molecule, $e^{'} = e - 36eV$, h is Planck's constant, ν is the frequency of the emitted wave and * denotes that it is excited. Every proton and electron can produce an ion pair per 36 eV of their initial energy.
Equation 2.4 is used to find the initial energy of the different wavelengths.

$$E = \frac{hc}{\lambda} \tag{2.4}$$

where c is the velocity of light and λ is the wavelength.
Each species emit a different emission line, and there can also be several emission lines associated with one species. Atomic oxygen can send out at least three emission lines after it is excited; for example 557.7 nm , 630.0 nm and 844.6 nm lines. The emission of each of these lines are dependent on how much the atomic oxygen is excited and the energy of the incoming particle. The emission lines are therefore dependent on the energy level after it is excited and the process from the excited state to the ground level state.

For atomic oxygen we have:

$$O(^3P) + e \rightarrow O(^1S) + e^{'} \tag{2.5}$$

$$O(^1S) \rightarrow O(^3P) + h\nu \tag{2.6}$$

where $h\nu$ is the emission line 557.7 nm.

This means that the atomic oxygen will be excited from level ^3P to ^1S, see Equations 2.5 and 2.6. After the lifetime of the excited state, it will emit green light, 557.7 nm line [Omholt, 1973]. The lifetime is dependent on the number of particles at its altitude and intensity of the emission line which in this case is around 0.7 seconds. Because this is such a short time, the aurora would look bright and have structures which are visible with the naked eye. The initial energy of the wavelength will be 2.22 eV from equation 2.4, but they need 4.2 eV to be excited [Brekke, 2012].

For the red line, the process is

$$O(^3P) + e \rightarrow O(^1D) + e^{'} \tag{2.7}$$

$$O(^1D) \rightarrow O(^3P) + h\nu \tag{2.8}$$

where $h\nu$ is the emission line 630.0 nm.

The atomic oxygen will here be excited from level ^3P to ^1D shown with equations 2.7 and 2.8. After the lifetime of the excited state, it will emit red light [Omholt, 1973]. Since the lifetime is 110 seconds, it would look like diffuse red aurora, because the excited particles travel a great distance before they emit light. The initial energy will be 1.97 eV from equation 2.4. Emission 630.0 nm line needs 2 eV to be excited [Brekke, 2012].

The 844.6 nm line goes from level $^3S_1^0$ to level $P^3_{2,1,0}$ [Brekke, 2012]. The lifetime is so prompt that we do not know how fast it is. It will send out near UV light. The initial energy will be 1.468 eV from equation 2.4. It needs less energy to be excited than the 630.0 nm line as expected due to the longer wavelength.

The process for N_2 is described as

$$N_2 + e \rightarrow (N_2^+)^* + (e - 36eV) \tag{2.9}$$

$$N_2 + H^+ \rightarrow (N_2^+)^* + (H^+ - 36eV) \tag{2.10}$$

$$(N_2^+)^* \rightarrow N_2^+ + h\nu \tag{2.11}$$

where $h\nu$ is the emission lines 391.4 nm and 427.8 nm. The 394.1 nm line is not the focus in this thesis due to lack of observations.

The 427.8 nm emission line is from N_2^+ where the photon excites the vibration level. It goes from vibration level $B^2\Sigma^+_{upperstate}$ to vibration level $X^2\Sigma^+_{ground}$ [Brekke, 2012]. It will emit blue lights after the lifetime. The wavelength initial energy will be 2.90 eV from equation 2.4. The emission line needs 18.75 eV to be excited. This process needs more energy to produce the emission line than the other processes mentioned above [Brekke, 2012].

2.2.4 Height of the Spectral Emissions

The height of the spectral emissions is dependent on the energy of the particles and the density in the Earth's atmosphere. Particles from the solar wind will collide with the constituents of the atmosphere until their energy is too low to cause ionization and excitation. They will come to rest in the atmosphere. The height is also related to the pitch angle distribution of the particles [**?**]

Carl Størmer found a way to detect the height of the spectral emissions. It was by using triangulation [Brekke, 2012]. Carl Størmer measured 12330 auroral points [Carlson Jr. and Egeland, 1995], and from this he found that the height of the aurora was between 90 km and 250 km. Now we measure it with sensible light gauges in rockets or with radars [Lorentzen, 2007].

The different wavelengths appear with different height distributions. For night-time aurora, the 557.7 nm line is from 100 km to 250 km and has an intensity peak at 140 km. The 630.0 nm line goes from 160 km to 300 km, and have peak intensity at 260 km. The 427.8 nm line goes from 100 km to 250 km and have peak intensity around 140 km [Carlson Jr. and Egeland, 1995].

The 844.6 nm line has not been investigated much compared to the other lines mentioned, but it will have a higher altitude than the 630.0 nm line since it needs less energy to be excited.

2.3 Incoherent Scatter

Incoherent scatter is a weak scatter resulting from high-frequency electromagnetic waves that accelerate electrons in the ionosphere [Schunk and Nagy, 2009, Sulzer, 2003]. The ions can also be accelerated and scatter, but they are not as good as the electrons because of their high mass compared to the electrons. The accelerated electrons emit radiations, and some of this is detected by an incoherent scatter radar. The radar equation describes the received power:

$$P_r = P_t \sigma_{radar} \frac{G_t}{4\pi R_i^2} V \frac{A_{rec}}{4\pi R_s^2} \tag{2.12}$$

where P_t is the transmitted power, σ_{radar} is the radar scattering cross section, G_t is the gain of the transmitting antenna, A_{rec} is the effective area of the receiving antenna, V is the scattering volume, R_i is the range to the scattering volume from the transmitter and R_s is the range from the scattering volume

from the receiver [Hagfors, 1975].

The received spectrum is dependent on the Debye length and the pulse wavelength. If the Debye length is larger than the pulse wavelength, the radar will only see the velocity distribution of the electrons often described as Thomson electron scatter [Sulzer, 2003, Bjørnå, 2005].

If the Debye length is much smaller than the pulse wavelength, the radar will detect the ions and their cloud of electrons. It is then possible to get information about both the ions and the electrons, see e.g Sulzer [2003], Bjørnå [2005].

Because the ions have a more significant mass than electrons, we may assume that the ions are stationary. Since ions attract electrons, the electrons will follow the motions of the ions. The power spectrum shown in Figure 2.4 gives us information about the properties of the ions. The shape of the received power spectrum is dependent upon the dispersion relation of the ion-acoustic waves.
The waves are Landau damped and the dispersion relation is:

$$\omega_c = \frac{kC_s}{1 + k^2\lambda_e^2} \tag{2.13}$$

where k is the wave number, λ_e is the Debye length of the electrons, C_s is the ion-sound speed and it is given by

$$C_s = \left(\frac{\gamma_e k_b T_e + \gamma_i k_b T_i}{m_i}\right)^{\frac{1}{2}} \tag{2.14}$$

where k_b is the Boltzmann constant, T_e is the electron temperature, T_i is the ion temperature, m_i is the ion mass, γ_i is adiabatic lapse rate for ions and γ_e is the adiabatic lapse rate for electrons.

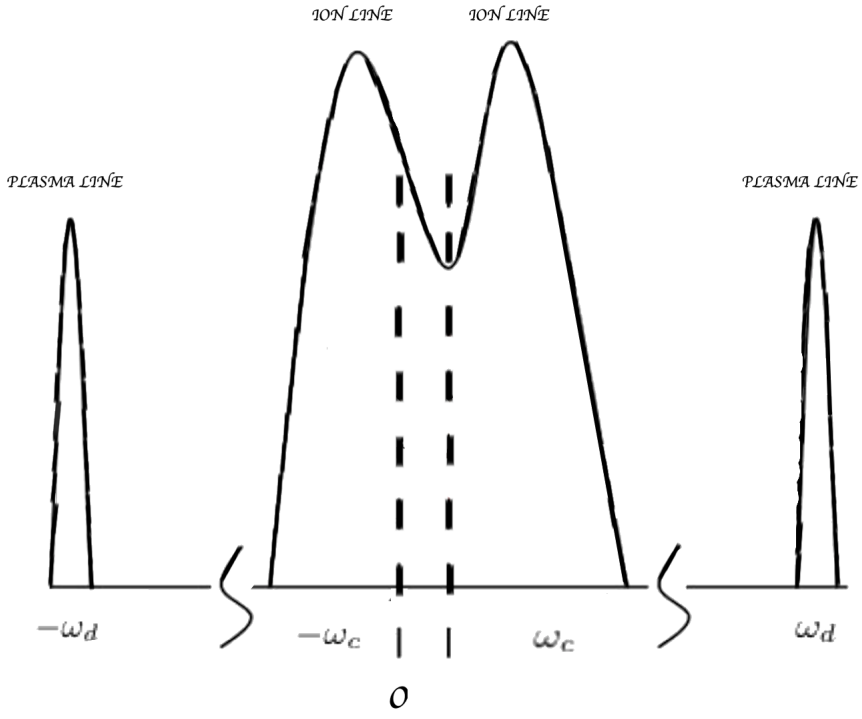

Figure 2.4: An incoherent scatter power spectrum with the plasma lines and ion lines. ω_c is the ion acoustic wave given by equation 2.13 and ω is the Langmuir wave given by equation 2.15. Based on Lunde [2009].

It is possible to find the temperature of the ions and electrons, electron density and the line-of-sight velocity by investigating the power spectrum shown in Figure 2.4.

The plasma lines in the power spectrum represent the Langmuir waves. The dispersion relation is given by

$$\omega = \left(\omega_{pe}^2 + 3k^2 v_{th,e}^2\right)^{\frac{1}{2}} \tag{2.15}$$

where ω_{pe} is the electron plasma frequency, $v_{th,e}$ is the electron thermal velocity and k is the wave number.

2.4 Naturally Enhanced Ion Acoustic Lines

Naturally Enhanced Ion Acoustic Lines (NEIALs) is a phenomenon that can be observed in the incoherent scatter spectrum where one or both shoulders are enhanced. The first time it was observed in the cusp/cleft region by the EISCAT Svalbard Radar was by Buchert et al. [1999]. NEIALs are believed to be a more common phenomenon in the ionospheric upper F layer, from around 300 km to 700 km. However, they have also been detected at both lower and higher altitudes. [Lunde et al., 2007]

NEIALs are associated with intense red aurora [Collis et al., 1991], high electron temperature [Wahlund et al., 1992], soft precipitation [Collis et al., 1991], electron density enhancement in the E-region [Rietveld et al., 1991] and severe geomagnetic disturbances [Rietveld et al., 1991].

Severe geomagnetic disturbances have a K_p index value above 4 and geomagnetic variations up to around 500 nT or more. Rietveld et al. [1991] observed at higher altitudes, above 450 km, that the left shoulder was more enhanced than the right shoulder. Collis et al. [1991] measured red aurora as intensive as 270 kR, but most of the time, the high red aurora intensity was between 10 kR and 40 kR. The red intensity has to be above 10 kR [Collis et al., 1991], and the intensity of the ratio of the red line and the green line needs to be above 5 [Lunde et al., 2007]. Lunde et al. [2009] argued that the 844.6 nm line is a better choice as an indicator of NEIAL activity than the 630.0 nm line. Both the 630.0 nm line and the 844.6 nm line are associated with soft particle precipitation [Lunde et al., 2009]. It correlates well with Collis et al. [1991].

The 557.7 nm line is associated with the night time aurora, and precipitation of particles in the night time typically have energies between 1 keV and 15 keV [Omholt, 1973]. The height of the 557.7 nm emission is lower than 630.0 nm emission, and we can see that more energy is needed to penetrate to lower altitudes. Therefore the 557.7 nm line is associated with medium energy electron precipitation.

NEIALs are not frequently observed and Grydeland [2003] suggested that NEIALs happen within a few tenths of a second. To find NEIALs in the EISCAT quick-look plots, we need to see an increased electron temperature which should be higher than the ion temperature [Wahlund et al., 1992], typically a factor of three or more. The other properties are to have an increased electron density with a distinct structure, and a noticeable ion up or in flow.

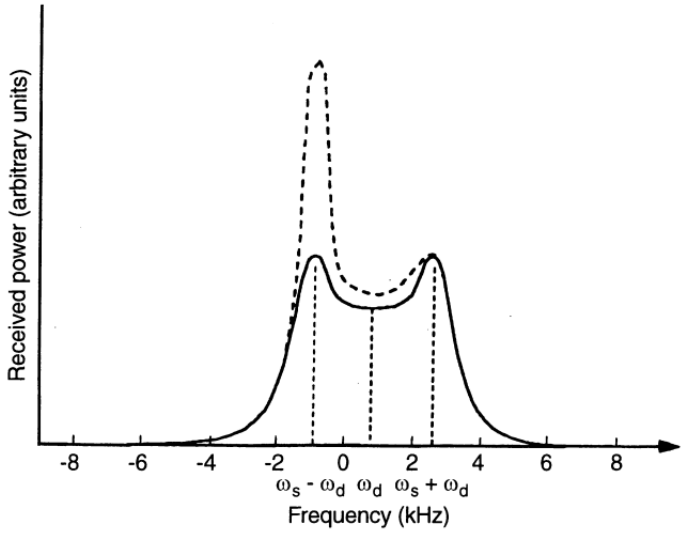

Figure 2.5: The incoherent scatter spectra. The solid line represents a double humped shape as from Figure 2.4 . The dashed line is a power spectra with an enhancement in the left shoulder. The ω_s is the ion acoustic frequency, ω_d is the Doppler shift. Courtesy Forme and Fontaine [1999].

An example of NEIAL is shown in Figure 2.5.

Why NEIALs occur, and the physical mechanism of this phenomenon is not well understood. However, there have been three important theories which are suggested to explain NEIALs. These are the current driven instability [Rietveld et al., 1991], ion-ion two-stream instability [Wahlund et al., 1992] and parametric decay of Langmuir waves [Forme, 1993].

2.4.1 Current Driven Instability

Rosenbluth and Rostoker [1962] was the first to suggest that field-aligned currents enhance the incoherent scatter spectrum. Rietveld et al. [1991] observed this enhancement and argued that the enhancement was due to a strong field-aligned current carried by thermal electrons as Rosenbluth and Rostoker [1962] first suggested. However, the field-aligned current density needed to be higher than was measured up to that time, in order of mAm^{-2}. It was not until 2003 that the Ørsted Satellite measured such large current densities [Neubert and Christiansen, 2003]. Differences between electron and ion drifts cause enhancement in one of the shoulders in the incoherent scatter spectrum. This theory does not explain the enhancement of both shoulders simultaneously.

2.4.2 Ion-Ion Two-Stream Instability

Wahlund et al. [1992] argued that there were no observations of the high electron currents densities required for the current driven instability, and therefore believed that ion instabilities could produce NEIALs. A large drift velocity between two or more ion species produces this instability [Wahlund et al., 1992]. This theory can explain that there is an enhancement in both shoulders, but the drift velocity needs to be higher than the species thermal velocity [Wahlund et al., 1992]. Because of the high drift velocity, NEIALs will probably not occur at lower altitudes. It is because the drift needs a high acceleration of H^+, which may occur at higher altitudes than the F-layer.

2.4.3 Parametric Decay of Langmuir Waves

This theory does not require a high current or large relative drift velocities. Parametric decay of Langmuir waves theory is about a beam of electrons with energy from 10 eV to 500 eV which produces a bump on the tail of the electron velocity distribution [Forme, 1993]. This leads to an excitation of the Langmuir waves that makes secondary ion acoustic waves. NEIALs are not likely to occur during more energetic precipitation according to this theory [Forme, 1993]. Therefore this theory is associated with the 630.0 nm line and the 844.6 nm line. These types of emission lines are produced by soft particle precipitation.

3

Instrumentation

3.1 EISCAT

EISCAT (European Incoherent Scatter) is a research foundation which runs three radar systems located in the northern Fenno-Scandinavia and in Svalbard, with the aim at studying the ionosphere. The EISCAT facilities in Svalbard is a system with two antennae with a 500 MHz transmitter. One of the antennae is a 32 meter steerable parabolic antenna, and the other one is a 42 meter parabolic antenna that is fixed in the field-aligned direction. The EISCAT Svalbard Radar (ESR) is located in Longyearbyen at 78.15 ° North and 16.03 ° East geographic coordinates. See Wannberg et al. [1997] for further descriptions of the ESR system. The corrected geomagnetic latitude and longitude are 75.4° latitude and 110.68° longitude, respectively. In this thesis, we will focus on data from the 42 m antenna which has a tangent to the geomagnetic field at around 300 km. The antenna is pointing in 182.2° azimuth and 81.6° elevation which is the same position that we use for the data from the Meridian Scanning Photometer.

The parameters measured by the EISCAT radar systems are the electron density, electron and ion temperatures and line-of-sight velocity, however, different experiments are used depending upon range resolution, time resolution and position in space. The ESR system has nine experiments. These experiments are named arc slice, hilde, steffe, taro, manda, ipy, beate, folke and tau0. Each experiment has a different type of instructions.

3.2 Meridian Scanning Photometer

Meridian Scanning Photometer (MSP) is a small instrument that measures the intensity of the different wavelengths in the aurora. The intensity is measured in Rayleigh, which is a unit for photon flux and emission rate.

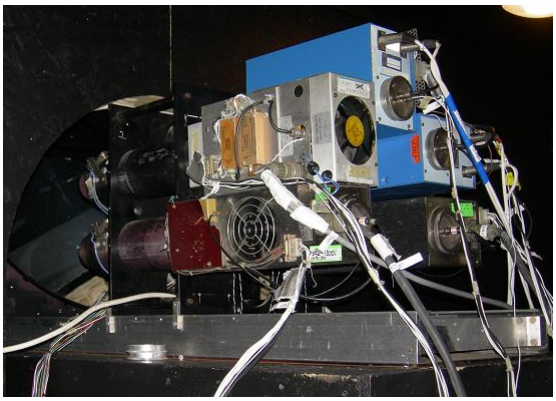

Figure 3.1: The MSP instrument. Courtesy Lorentzen [2002].

The MSP shown in Figure 3.1 is designed such that there is a rotating mirror that scans the sky from 10 degrees elevation in the north to 10 degrees elevation in the south along the magnetic meridian [Sigernes et al., 2002]. The MSP has five channels, where each channel has a bandpass filter such that they can measure one auroral emission wavelength per channel. It scans 180 degrees every 16 seconds [Sigernes et al., 2002].

There is one MSP located at the Kjell Henriksen Observatory in Svalbard. However, during our selected days the MSP was installed at the Auroral Station in Adventdalen, which is located seven km from the EISCAT facilities. In this thesis we have chosen four wavelengths from the MSP measurements. These emission lines are the 557.7 nm, the 630.0 nm and the 844.6 nm from atomic oxygen and the 427.8 nm line from dinitrogen ions.
One of the emission lines that are included in the MSP is the 486.1 nm line, but because there is no correlation between this emission line with NEIALs, we will not include this further.

3.3 Magnetometer

The Magnetometer is an instrument that measures the magnetic field strength and direction of the Earth's magnetic field. Energetic particles that penetrate the Earth's atmosphere create a magnetic field that affects the Earth's magnetic field. The induced magnetic field will create a disturbance in the Earth's magnetic field which is shown in a magnetometer plot. There are two basic types of magnetometers. There is the vector magnetometer that measures the magnetic field vector component and orientation, and the other one measures the magnitude. In this thesis, the Auroral Station magnetometer, which is a fluxgate magnetometer, is used. Fluxgate is a vector magnetometer which measures the magnetic field components H, D and Z. The horizontal direction (H) is the most used component to identify the disturbances in the magnetic field and was therefore chosen. The magnetometer data in this thesis is used to determine if there is geomagnetic activity associated with the NEIAL events.

4

Observations and Results

To asses if there is a geomagnetic activity such as a substorm or storm, indices are used. There are several indices to describe the geomagnetic activity of the Earth. The K_p index gives information about the geomagnetic activity on the globe. D_{st} is a geomagnetic storm index and reveals if there is a substorm or geomagnetic storm.

AE (Auroral Electrojet Index) is a global index that measures the auroral zone magnetic activity. The most important index is the IE index, which is the difference between the maximum and the minimum variation of the geographic north component of the magnetic field. The IE index describes the auroral electrojet activity for a time zone.

Index	Quiet-minor	Moderate storm	Intense storm	Superintense storm
D_{st} [nT]	> -50	-50--100	<-100	<-250
K_p	0-4	5	7-9	

Table 4.1: The thresholds for the geomagnetic activity for K_p and D_{st}. Based on Palacios et al. [2017].

Table 4.1 describes the different threshold for the geomagnetic activity indices. For the AE and the IE indices, there has been described that values over 100 nT gives a moderate geomagnetic activity. The AE index has been measured up to 1000 nT.

The days presented in this thesis are 2000 – 11 – 27 , 2001 – 11 – 16, 2003 – 12 – 20 and 2004 – 01 – 22. These days were found by analyzing the quick-look plot on the EISCAT web page and was chosen because there was a structure in the increased electron density, increased electron temperature and ion out or inflow. We then checked if good quality MSP data was available.

For all the chosen days, experiment tau0 was used. Tau0 is a 16 bit alternating code experiment with a covering of altitudes between 53 km to 1297 km. It has a sampling interval of 20 μs, and 6.4 s time resolution [Tjulin, 2015].

To identify NEIALs in the EISCAT data, functions were created in MATLAB to plot the ion lines. We integrated with GUISDAP (Grand Unified Incoherent Scatter Design and Analysis Package) with an integration time of 6.5 s because tau0 operates with this. These ion lines are represented in a $3D$ figure with height, frequency and power in the unit of decibel (dB).

Even though we integrated with an integration time of 6.5 s, some of the data presented here have an integration time of 13 s. The reason for this is because they used both antennas in the experiment and switched which antenna they used per 13 s. However, by choosing 6.5 s, these data will have the lowest integration time the experiment used.

The intensities of the auroral emission lines were found from the MSP data where we selected the position of the ESR 42 m antenna. The intensities are shown in a $2D$ plot, where each color corresponds to one emission line.

The dates 2000 – 11 – 27 and 2004 – 01 – 22, have been presented with NEIALs and their correlation with the Meridian Scanning Photometer data from the PhD thesis to Lunde [2009]. We have extended the work to also look at different data dumps than Lunde [2009].

4.1 Observations and Results of the Experiment on 2003-12-20

On 2003 – 12 – 20, the geomagnetic activity was moderate with a K_p index of 3^+. The AE index was high between 9.30 UT and 12.00 UT. The D_{st} was at minimum of −21 nT. The IE index was high between 10.00 UT and 14.00 UT with a maximum of 250 nT at 11.00 UT. The interplanetary magnetic field component B_z became negative at 10.00 UT and positive between 11.00 UT and 12.00 UT. The magnetic field was switching between −10 nT and 10 nT. The solar wind was estimated to be 350 kms^{-1}. The space weather data provided give no indications of a geomagnetic storm or substorm during our time of interest.

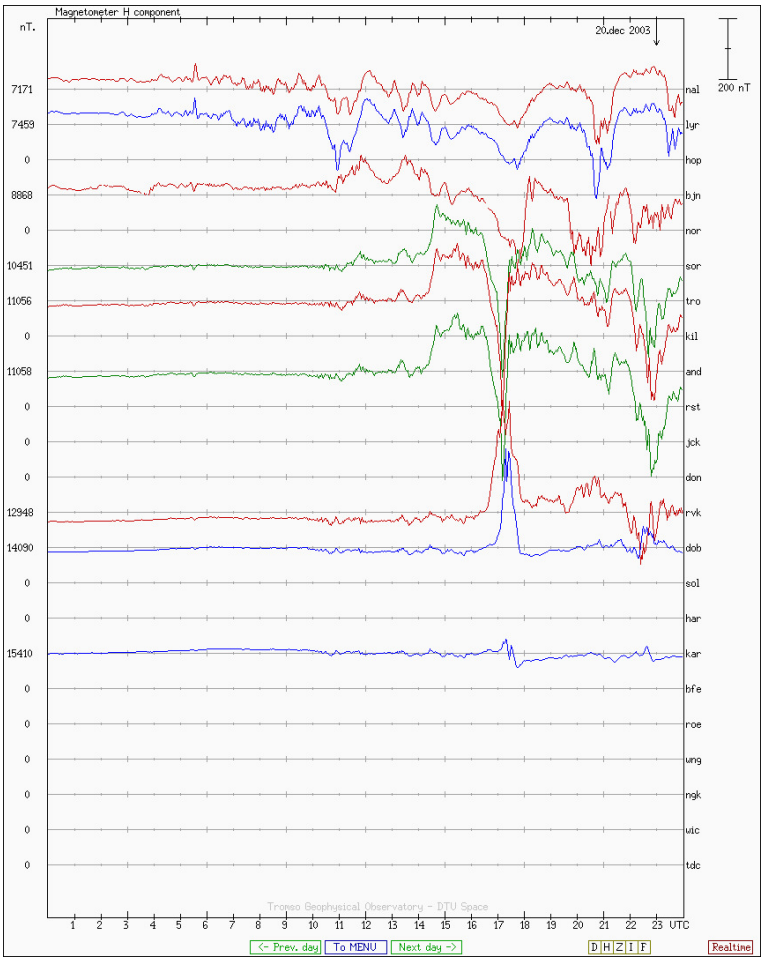

Figure 4.1: Magnetometers measurements of the H component along the Norwegian line at 2003 – 12 – 20. The second line (blue) is from Longyearbyen. Data from Tromsø Geophysical Observatory.

Figure 4.1 shows the magnetometer plot of the H component along the Norwegian line. Data from Longyearbyen is shown with the blue line, second from the top. It was observed a disturbance in the magnetic field at around 11.00 UT followed by small disturbances up to 18.00 UT.

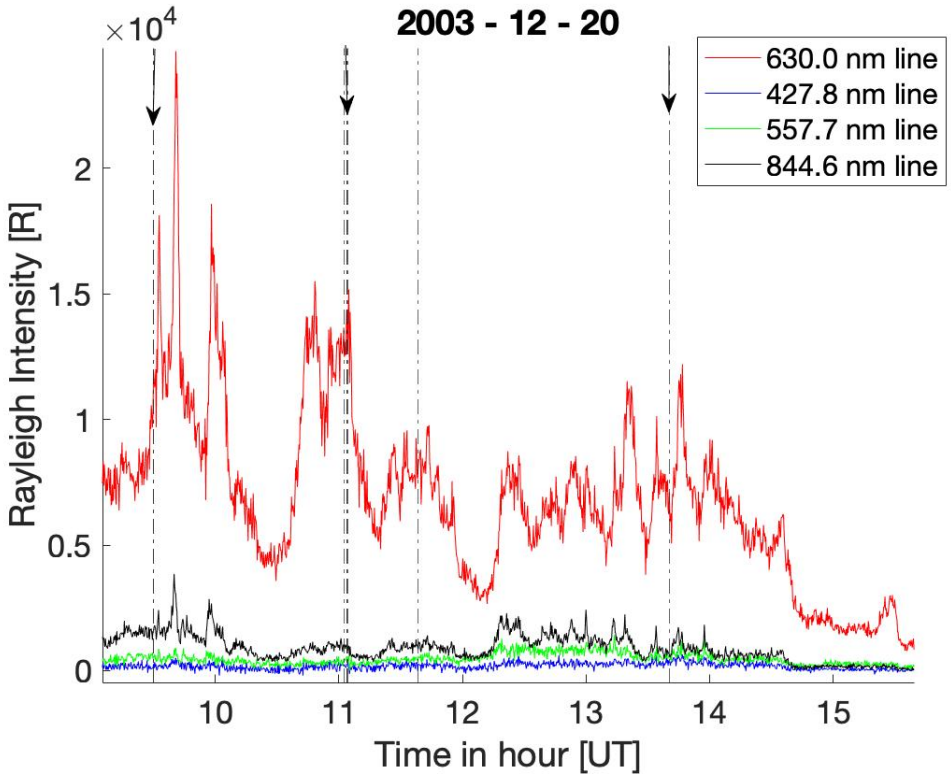

Figure 4.2: Data from the MSP from 2003 – 12 – 20. The dotted lines represent NEIALs, and the arrows indicate which NEIALs we are focusing on.

Figure 4.2 shows the intensity for the different emission lines where the dotted lines indicate NEIALs.

It was observed 15 NEIAL events. We selected four events and they occurred at 09.29.49 UT, 11.04.00 UT, 11.04.07 UT and 13.40.23 UT. The ion lines for the selected times are shown in Figure 4.3.

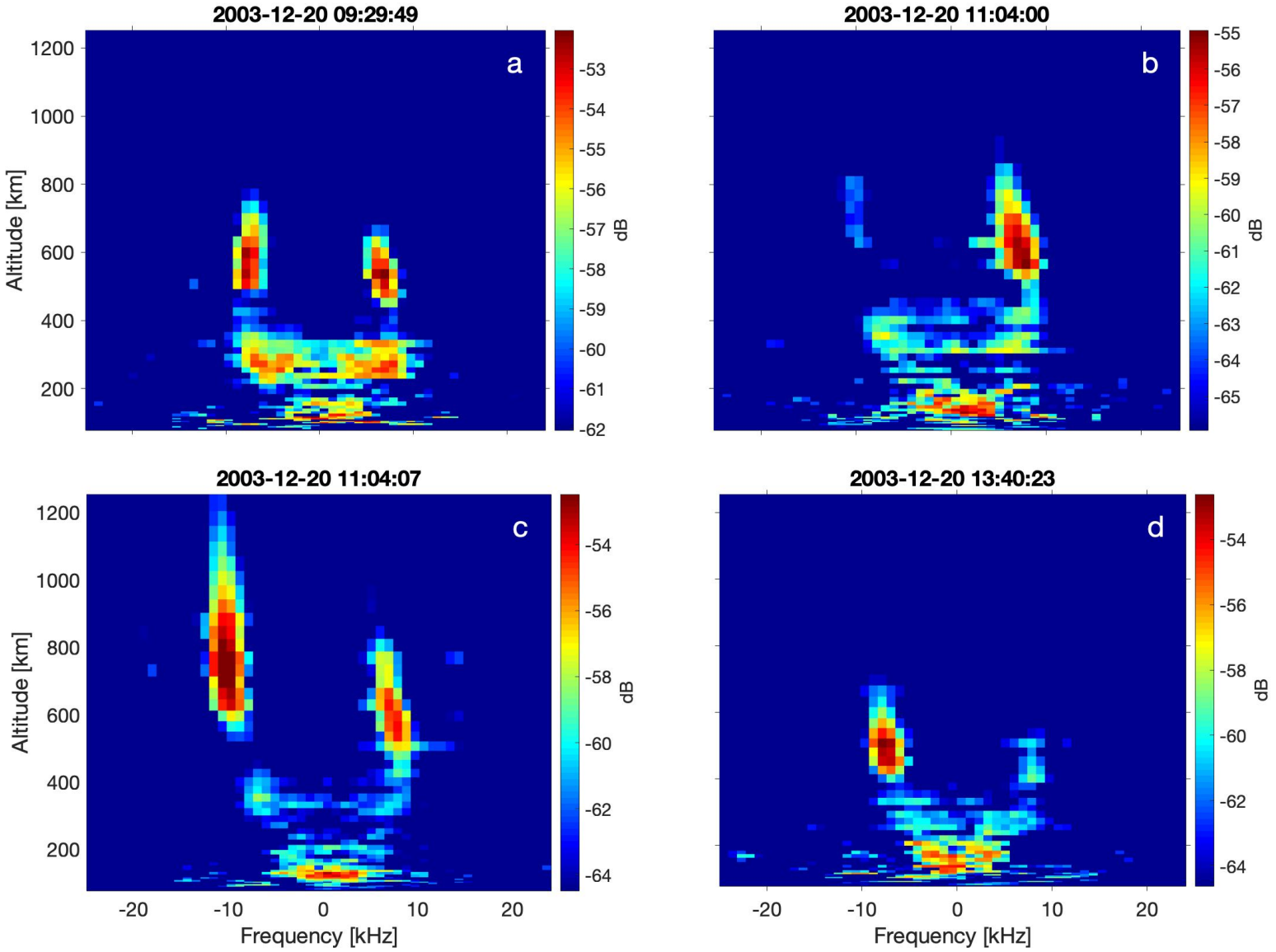

Figure 4.3: The NEIAL events shown with arrows in Figure 4.2. a) shows enhancements in both shoulders. b) shows an enhancement in the right shoulder. c) shows enhancements in both shoulders. d) shows an enhancement in the left shoulder.

Figure 4.3a shows enhancements in both shoulders. The left shoulder is enhanced from 500 km to 750 km and the right shoulder is enhanced from 450 km to 650 km. The intensities for the different lines were found from Figure 4.2. The intensity of the 630.0 nm line is 10.2 kR and the 557.7 nm line has an intensity of 468 R. The 844.6 nm line has an intensity of 1.6 kR and the 427.8 nm line has an intensity of 88 R.

There is an enhancement in the right shoulder from 500 km to 800 km shown in Figure 4.3b. There is also an enhancement in the left shoulder, but it is small compared to the right shoulder. The intensity of the 630.0 nm line is 13.7 kR, where the 557.7 nm line intensity is 556 R. The intensity of 844.6 nm line is 1.0 kR and for the 427.8 nm line the intensity is 231 R. The intensities were found from Figure 4.2.

From Figure 4.3c an enhancement in the left shoulder from 550 km to approximately 1200 km can be seen. The right shoulder is enhanced from 450 km to 800 km. The intensities for the emission lines were found from Figure 4.2. The intensity of the 630.0 nm line is between 13.7 kR and 12.7 kR, and the 557.7 nm line is between 556 R and 340 R. The 844.6 nm line is between 1.0 kR and 798 R. The 427.8 nm line has intensity between 231 R and 341 R.

From Figure 4.3d there is an enhancement in the right shoulder from 400 km to 650 km. At this time and from Figure 4.2, the intensity of the 630.0 nm line is 7.1 kR. The intensities of the 844.6 nm line and the 557.7 nm line are 665 R and 595 R, respectively. The 427.8 nm line has an intensity of 264 R.

4.2 Observations and Results of the Experiment on 2004-01-22

The D_{st} index was at minimum −130 nT, and the IE index was around 400 nT to 500 nT between 04.00 UT and 11.00 UT. The K_p index was around 5 during the time of interest. The AE index was high between 08.00 UT and 12.00 UT where the index was around 500 nT. The solar wind was relatively high (650 kms^{-1}) between 02.00 UT and 15.00 UT. The IMF B_z was low, around 5 nT. The IMF B_z was positive from 08.00 UT to 10.00 UT, and then negative at 11.00 UT. The selected time period for that day was from 08.00 UT to 12.00 UT. Both the D_{st} and IMF B_z indicate that a storm occurred during the time of interest.

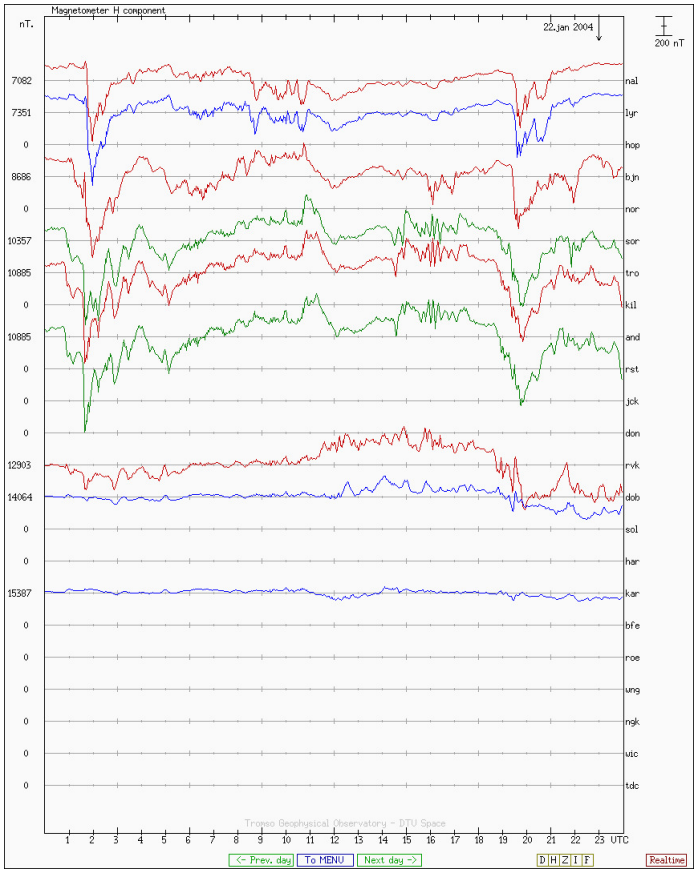

Figure 4.4: Magnetogram of the H component along the Norwegian line. The second line (blue) is from Longyearbyen. Data from Tromsø Geophysical Observatory.

In Figure 4.4 we see a disturbance in the H component around 02.00 UT. There

are small disturbances in the magnetic field between 08.00 UT and 10.00 UT which is the time of interest.

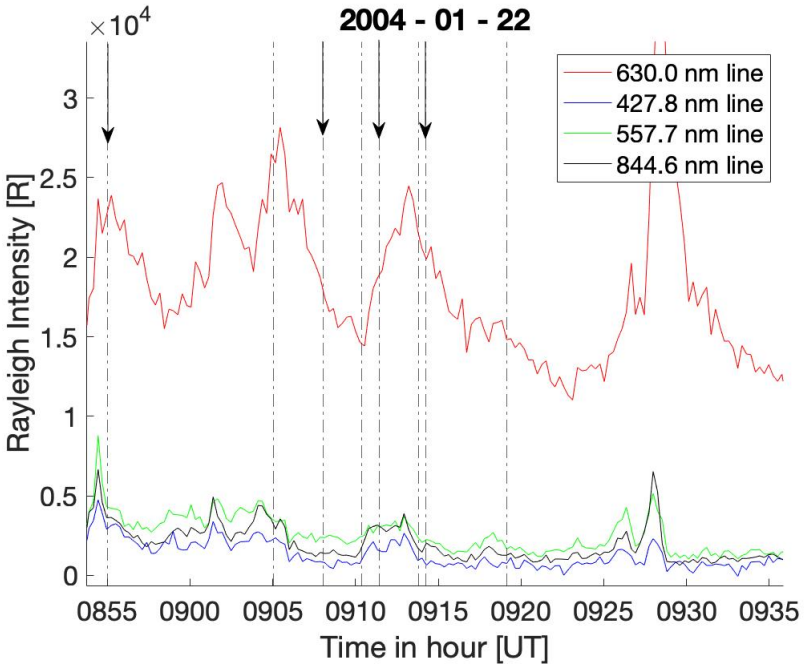

Figure 4.5: Data from the MSP for 2004 – 01 – 22. See Figure 4.2 for the description for the arrows and the dotted lines.

Figure 4.5 shows the intensities of the emission lines. The dotted lines represent the NEIAL events. In total there are 31 NEIAL events happening during the time period. The arrows are the NEIAL events selected and they occurred at 08.55.02 UT, 09.08.03 UT, 09.11.27 UT and 09.14.14 UT. The ion lines for these time events are shown in Figure 4.6.

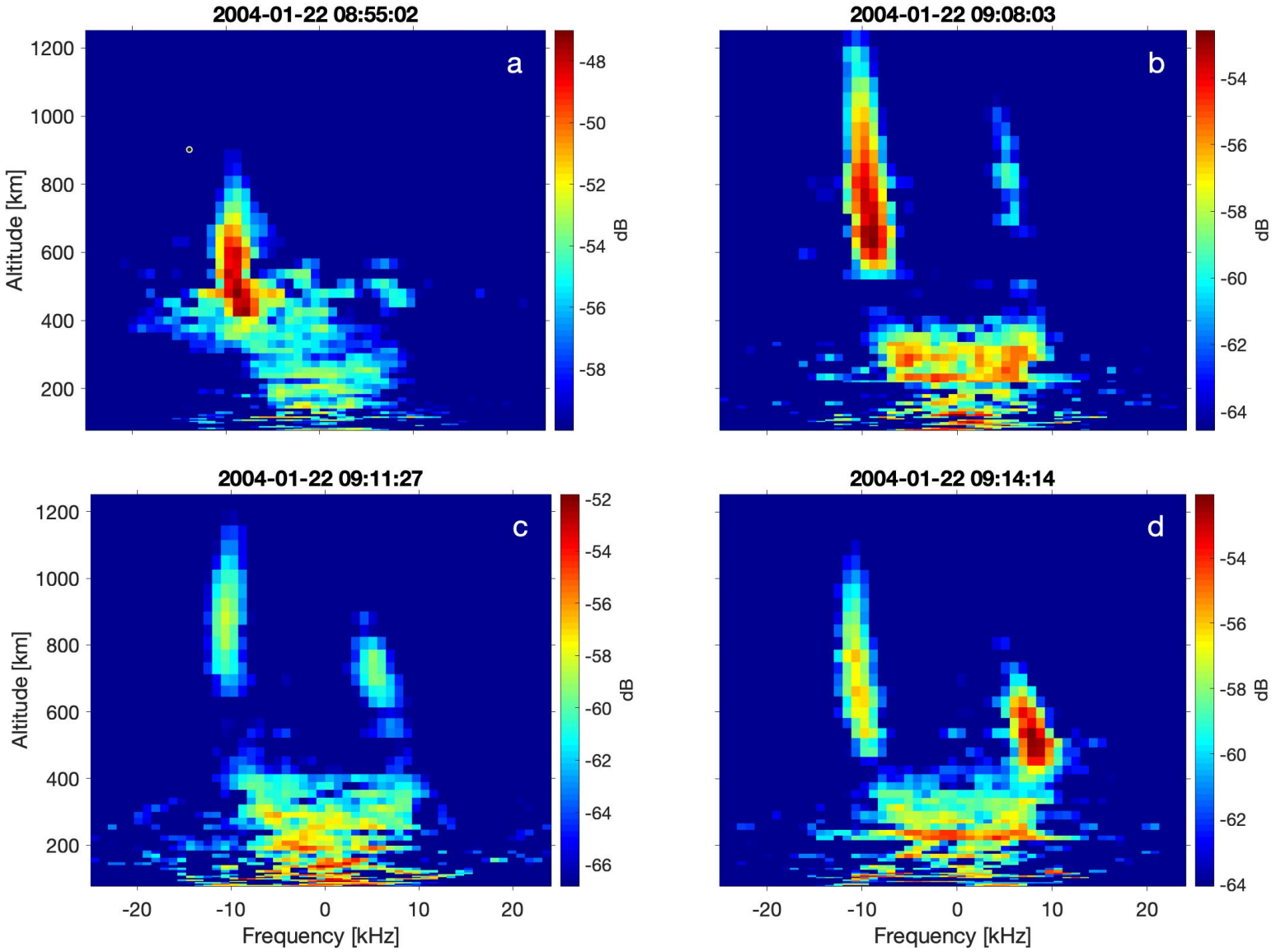

Figure 4.6: The NEIAL events from EISCAT data shown with arrows in Figure 4.5. a) shows an enhancement in the left shoulder. b) shows an enhancement in the left shoulder. c) shows enhancements in both shoulders. d) shows enhancements in both shoulders.

Figure 4.6a shows an enhancement in the left shoulder from 400 km to 800 km. From Figure 4.5 we can find the intensities for the different emission lines. For the 630.0 nm line the intensity is 22.7 kR, for the 844.6 nm line it is 3.6 kR, for the 577.7 nm line it is 4.3 kR and for the 427.8 nm line it is 2.9 kR.

There is an enhancement in the left shoulder at altitudes between 500 km and 1200 km, as shown in Figure 4.6b. Again, the intensities of the emission lines were found from Figure 4.5. The intensity is 19.5 kR for the 630.0 nm line. For the 844.6 nm line and the 557.7 nm line the intensities are 1.4 kR and 2.4 kR, respectively. For the 427.8 nm line the intensity is 803 R.

Figure 4.6c presents weak enhancements in both shoulders. The left shoulder is enhanced from 700 km to 1100 km and the right shoulder is enhanced from around 600 km to 850 km. From Figure 4.5, we can find the intensity for the different emission lines. The 630.0 nm line is between 18.7 kR and 19.2 kR. For the 844.6 nm line it is between 3.2 kR and 3.0 kR. The 557.7 nm line has an intensity of 3.1 kR. For the 427.8 nm line the intensity is between 1.6 kR and 1.5 kR.

There are enhancements in both shoulders, displayed in Figure 4.6d. At approximately 400 km to 650 km there is a very large enhancement in the right shoulder. From 450 km to 1100 km the left shoulder is enhanced. The left shoulder is more enhanced after 650 km compared to the right shoulder. The intensities were found from Figure 4.5. The intensity for the 630.0 nm line is 20.0 kR, for the 557.7 nm line it is 2.3 kR, for the 844.6 nm line it is 2.0 kR and for the 427.8 nm line it is 638 R.

4.3 Observations and Results of the Experiment on 2001-11-16

At $2001-11-16$ the K_p index was 2^+. The AE index was high at 14.00 UT, but otherwise quiet with a maximum of 300 nT. The D_{st} was at minimum with -33 nT. The IMF B_z was positive for almost the whole day. The value was between -5 nT and 15 nT. The IE index was under 100 nT between 00.00 UT and 06.00 UT. The IE index had a maximum at 12.00 UT of 200 nT. The solar wind was estimated to be 360 kms^{-1}. The IE index was under 100 nT. That day the selected time period was 03.00 UT to 06.00 UT and there is no indication of a storm or substorm in that time period.

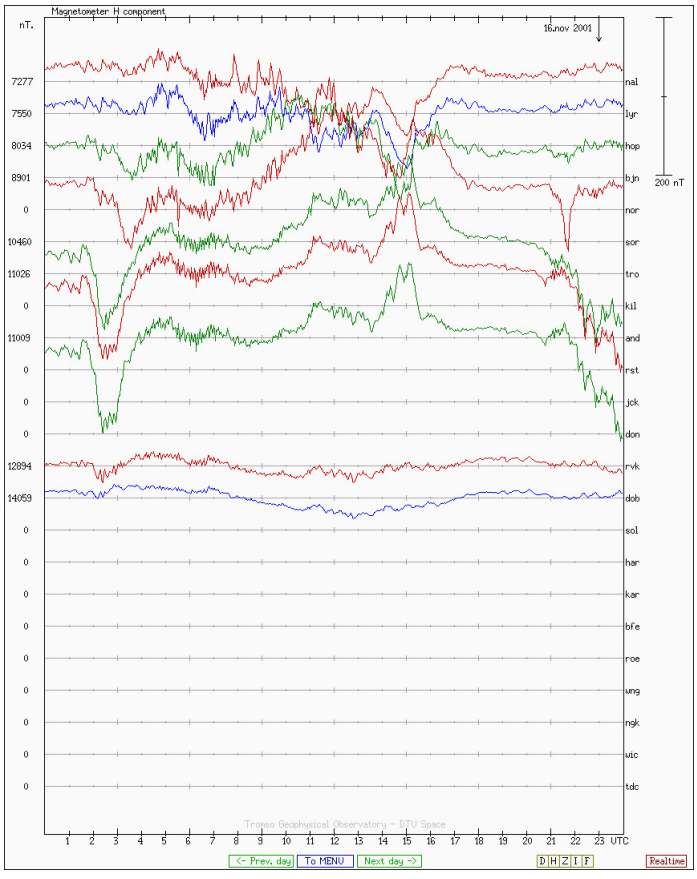

Figure 4.7: Magnetometers measurements for the H component along the Norwegian line for $2001-11-16$. The second line (blue line) is for Longyearbyen. Data from Tromsø Geophysical Observatory.

From the magnetogram shown in Figure 4.7, we can see that there are larger disturbances in the H component on the mainland compared to Longyearbyen.

There is a disturbance later at 15 UT, but not during the time of interest.

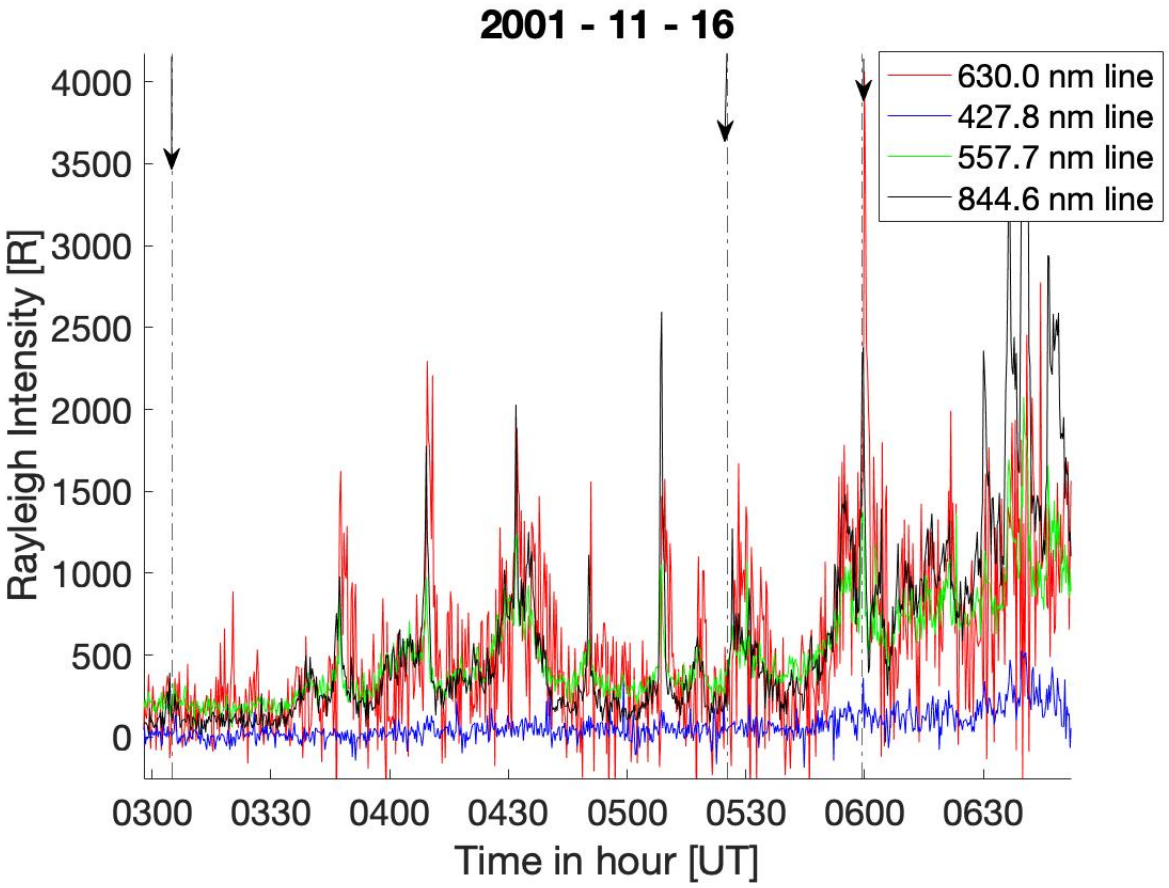

Figure 4.8: Data from the MSP at 2001 – 11 – 16. See figure 4.2 for the description of the arrows and the dotted lines.

Figure 4.8 shows the intensities of the emission lines. The dotted lines represent the NEIAL events which are the only ones found in the data set. The arrows indicate the NEIAL events at 03.05.08 UT, 05.25.18 UT and 05.59.20 UT. The ion line for these times are shown in Figure 4.10.

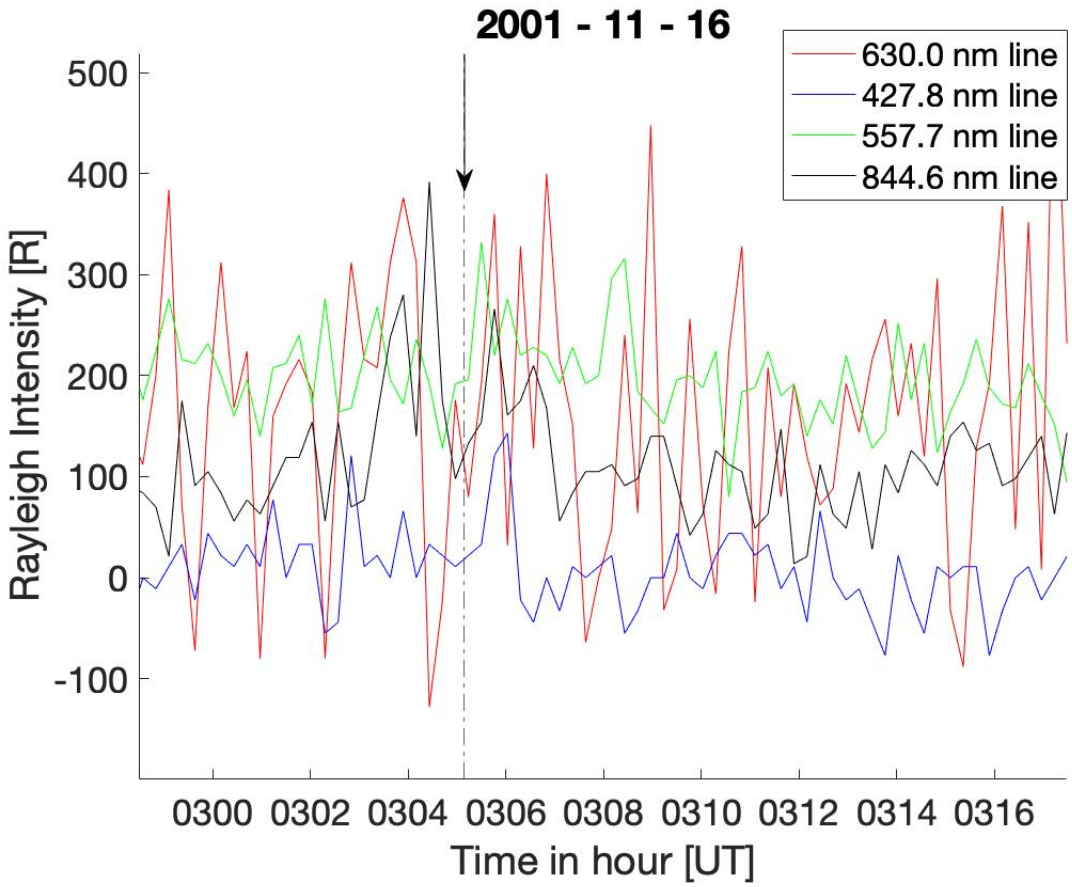

Figure 4.9: The intensity for the NEIAL events at 03.05.08 UT.

In order to increase visibility of the emission lines in Figure 4.8 we made an intensity plot for the time surrounding the first NEIAL. This is shown in Figure 4.9.

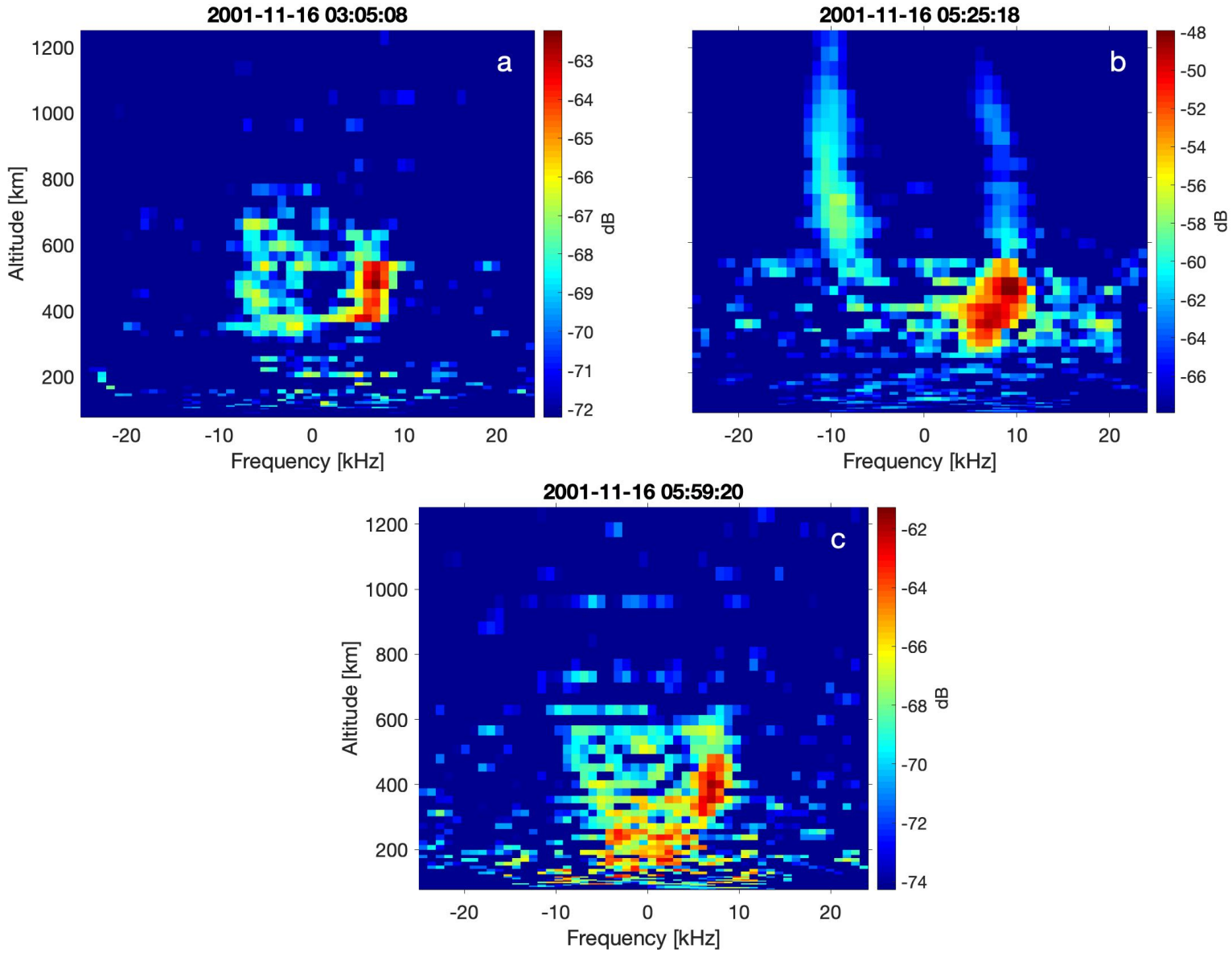

Figure 4.10: The NEIAL events shown with arrows in Figure 4.8. a) shows an enhancement in the right shoulder. b) shows enhancements in both shoulders. c) shows an enhancement in the right shoulder.

Figure 4.10a shows an enhancement in the right shoulder from 350 km to 550 km. In Figure 4.9 the intensities of the wavelengths are not very high compared to the other events. The 557.7 nm line has an intensity of 192 R. The 630.0 nm line has an intensity of 80 R, the 844.6 nm line has an intensity of 133 R and the 427.8 nm line has an intensity of 22 R.

Figure 4.10b shows an enhancement in the right shoulder from 300 km to 550 km. There is also an enhancement in the left shoulder from 500 km to over 1200 km. The left shoulder enhancement is weaker than the enhancement in the right shoulder. The intensities were found from Figure 4.8. For the 630.0 nm line the intensity is between 472 R and 200 R. The 557.7 nm line has an intensity between 436 R and 480 R and the 844.6 nm line has an intensity between 294 R and 364 R. The 427.8 nm line has an intensity between 33 R and 55 R.

There is an enhancement in the right shoulder from around 250 km to 500 km shown in Figure 4.10c. The intensity for the 630.0 nm line is 1.5 kR. For the 557.7 nm line and the 844.6 nm line the intensities are 1.4 kR and 2.3 kR, respectively. The 427.8 nm line has an intensity of 154 R. These intensities were found from Figure 4.8.

4.4 Observations and Results of the Experiment on 2000-11-27

During $2000-11-27$ the geomagnetic activity was moderate with a K_p index of 3^+. The AE index was high the whole day with a maximum of 1500 nT between 08.00 UT and 09.00 UT. Between 18.00 UT and 19.00 UT, the AE index was 1000 nT. The D_{st} index had a minimum of -80 nT. The solar wind was estimated to be 600 $kms-1$. The IMF B_z was switching between negative and positive. The IE index had a high peak at 01.00 UT with a value of 1000 nT. Otherwise, it was around 300 nT except approximately at 19.00 UT where the index became 700 nT. The D_{st} data show there was a storm.

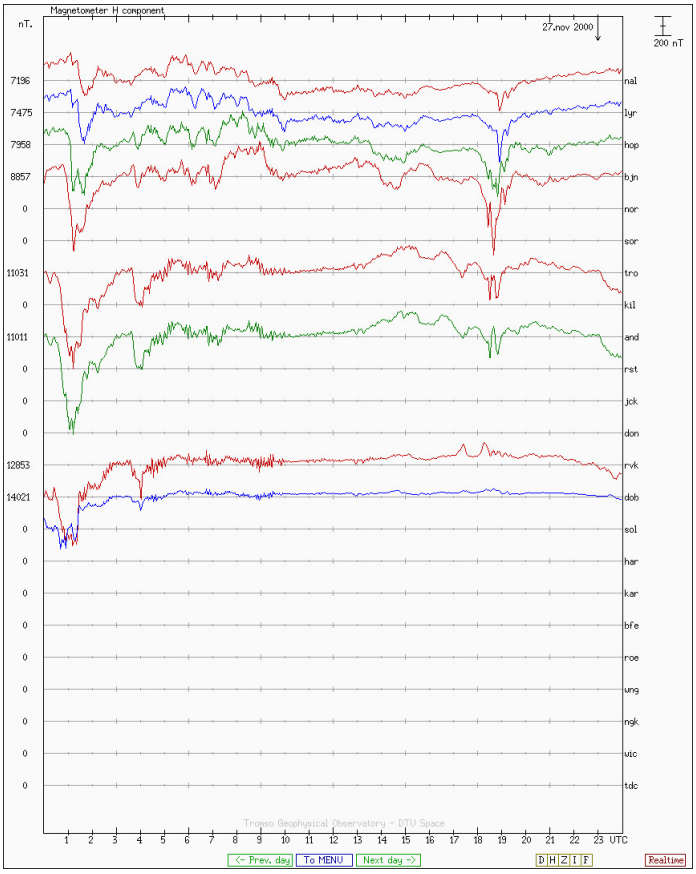

Figure 4.11: Magnetogram for the H component along the Norwegian line at $2000-11-27$. The second line (blue line) is from Longyearbyen. Data from Tromsø Geophysical Observatory.

Figure 4.11 shows disturbances in the H component of the magnetic field before

01.00 UT to 10.00 UT and negative excursions around 18.30 UT.

This day had 44 NEIAL events during the evening and the day. Day and night will be considered separately, because there is a time gap without NEIAL events from 12.30 UT to 19.00 UT.

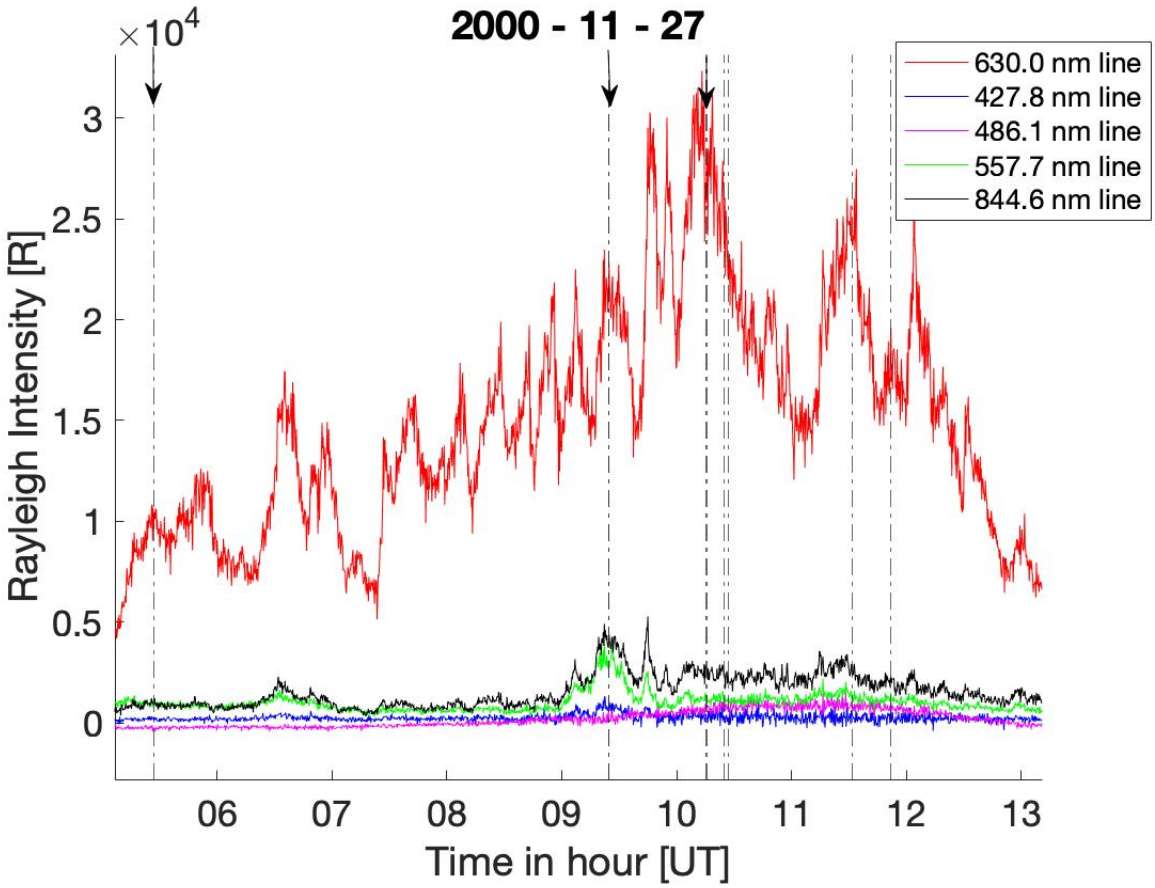

Figure 4.12: Data from the MSP at daytime of 2000 – 11 – 27. The description of the arrows and the dotted lines is explained in Figure 4.2.

During the daytime, we found 32 events of NEIALs and a selection of them are represented by the dotted lines in Figure 4.12. The arrows show the most interesting events of NEIALs; at 05.26.56 UT, 09.24.35 UT, 09.24.48 UT, 10.15.34 UT and 10.15.47 UT. The ion lines of these times are shown in Figure 4.13 and Figure 4.14.

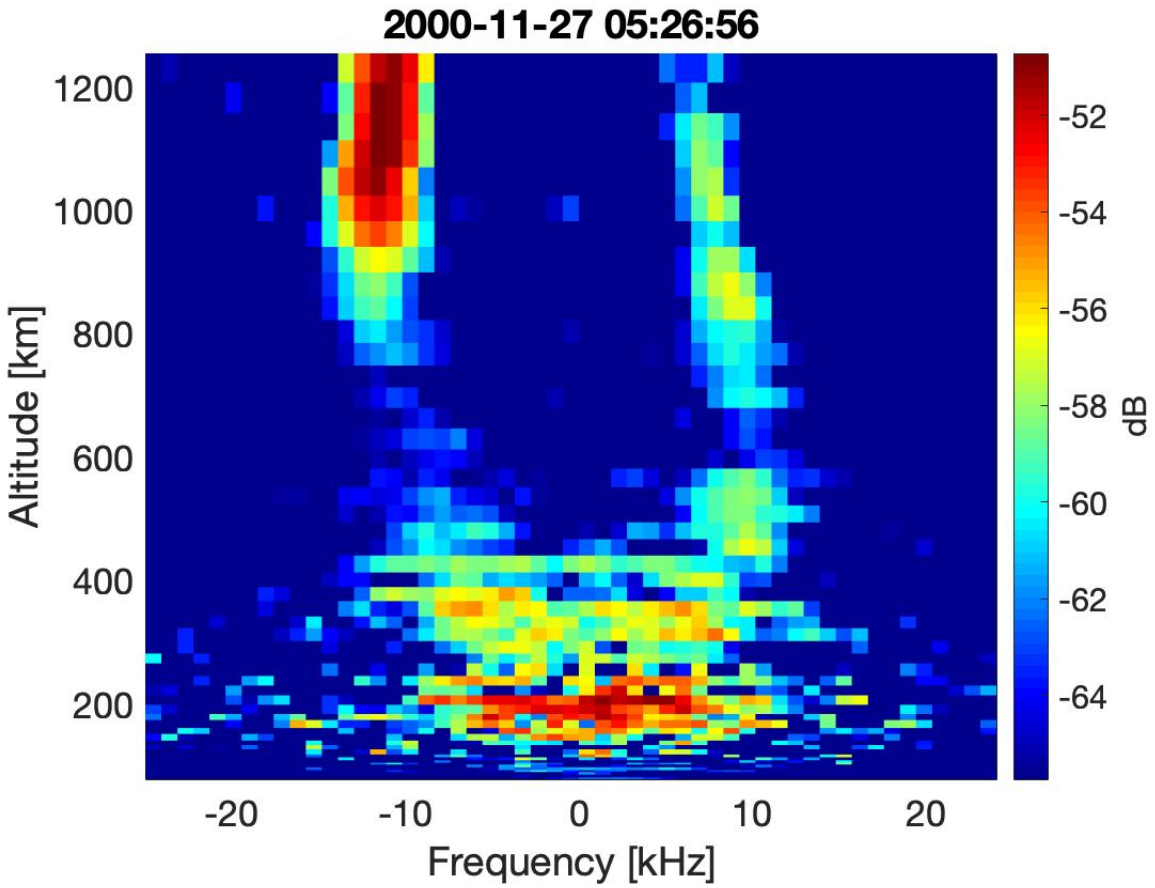

Figure 4.13: The NEIAL event with an enhancement in the left shoulder. A weak enhancement in the right shoulder can be seen as well.

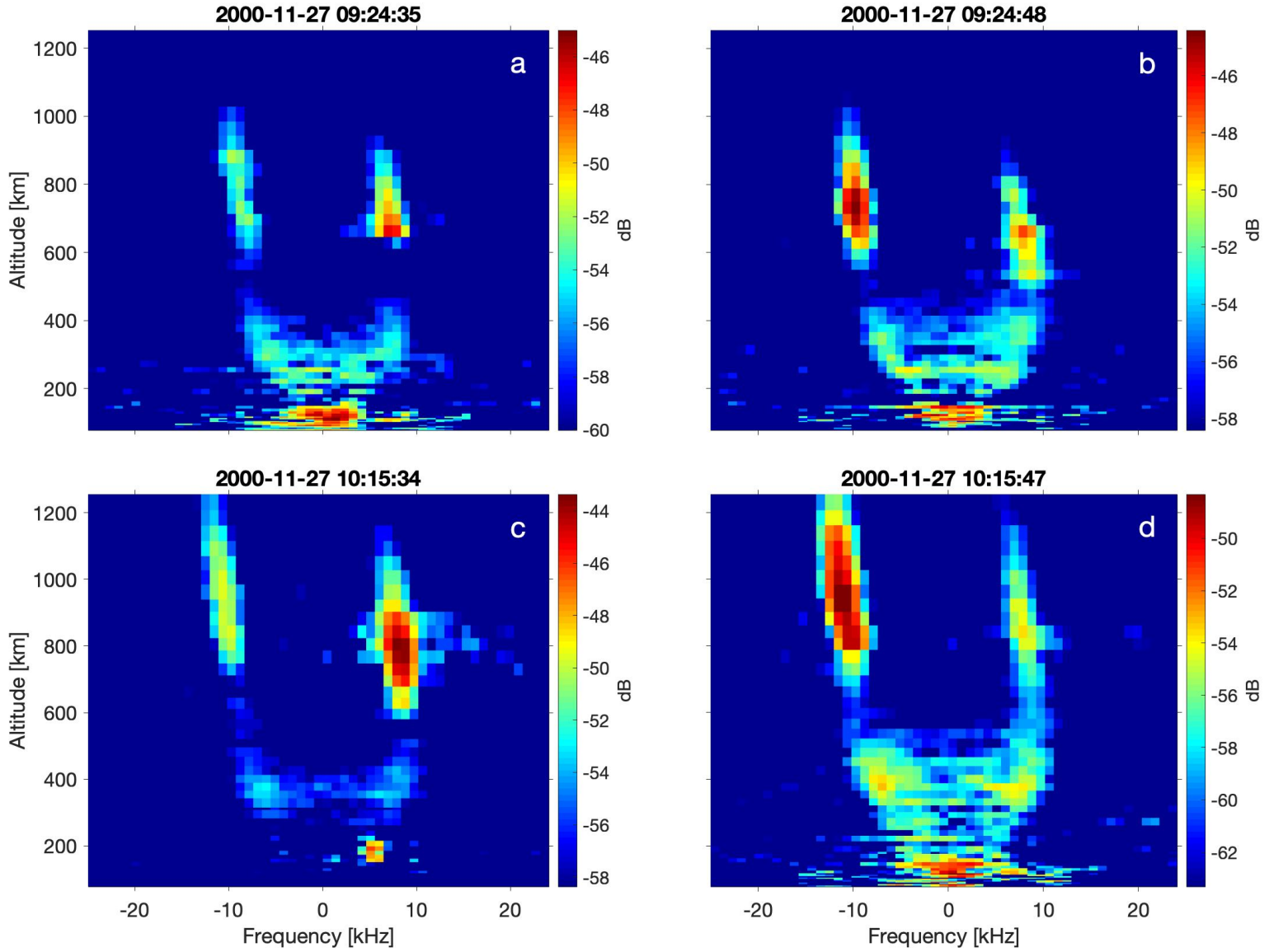

Figure 4.14: The NEIAL events shown with arrows in Figure 4.12. a) shows enhancements in both shoulders. b) shows enhancements in both shoulders. c) shows enhancements in both shoulders. d) shows enhancements in both shoulders.

There is an enhancement in the left shoulder from around 850 km to above 1200 km shown in Figure 4.13. The intensity for the 630.0 nm line was 9.6 kR, for the 557.7 nm line the intensity was 1.1 kR. The intensities for the 844.6 nm line and the 427.8 nm line were 1.1 kR and 154 R, respectively. These intensities were found from Figure 4.12.

In Figure 4.14a an enhancement in the right shoulder from 650 km to 800 km can be seen. There is an enhancement in the left shoulder from 600 km to 1000 km. The left shoulder is less enhanced compared to the right shoulder. The intensities were found from Figure 4.12. The intensity of the 630.0 nm line was 22.8 kR. The intensity of the 557.7 nm line and the 844.6 nm line were 3.0 kR and 4.4 kR, respectively. The 427.8 nm line had an intensity of 1.0 kR.

There is an enhancement in the left shoulder from 600 km to 1000 km shown in Figure 4.14b. There is an enhancement in the right shoulder from 500 km to 800 km. Again, the intensities for the different emission lines were found from Figure 4.12. The 630.0 nm line had an intensity between 23.0 kR and 21.6 kR, the 557.7 nm line between 3.0 kR and 2.7 kR, the 844.6 nm line between 4.4 kR and 4.1 kR and the 427.8 nm line between 1.0 kR and 979 R.

There is an enhancement in the right shoulder from 600 km to around 1050 km shown in Figure 4.14c. The left shoulder is also enhanced from around 750 km to above 1200 km. The enhancement in the left shoulder is weaker than the enhancement in the right shoulder. The intensities of the emission lines were found out from Figure 4.12. The 630.0 nm line was between 25.8 kR and 28.8 kR. The 557.7 nm line was between 1.4 kR and 1.2 kR. The 844.6 nm line was between 2.8 kR and 2.7 kR. For the 427.8 nm line the intensity was between 396 R and 220 R.

Figure 4.14d shows an enhancement in the left shoulder from 800 km to above 1200 km. The right shoulder is also enhanced from around 500 km to 1050 km, but is weaker than the enhancement in the left shoulder. This is the next data dump after Figure 4.14c. Again, the intensities were found from Figure 4.12. The 630.0 nm line intensity was between 28.8 kR and 27.2 kR, the 557.7 nm line intensity was 1.2 kR, the 844.6 nm line intensity was between 2.7 kR and 2.5 kR. The 427.8 nm line had an intensity between 220 R and 308 R.

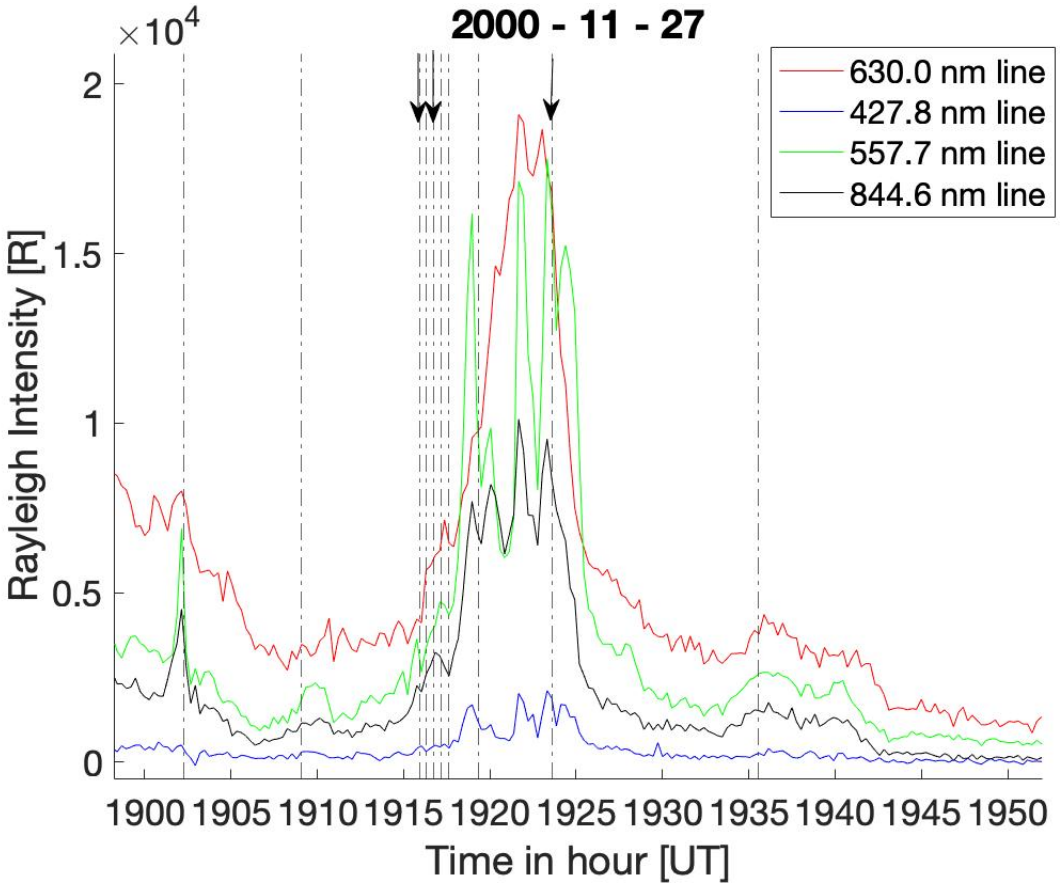

Figure 4.15: Data from the MSP for the evening of 2000 − 11 − 27. The dotted line and the arrows are explained in Figure 4.2.

Figure 4.15 displays the 12 NEIAL events found after 19.00 UT. These events are represented by the dotted lines. We selected three events shown with arrows in Figure 4.15 and they occurred at 19.15.55 UT, 19.16.46 UT and 19.23.36 UT. The ion acoustic lines for these events are shown in Figure 4.16.

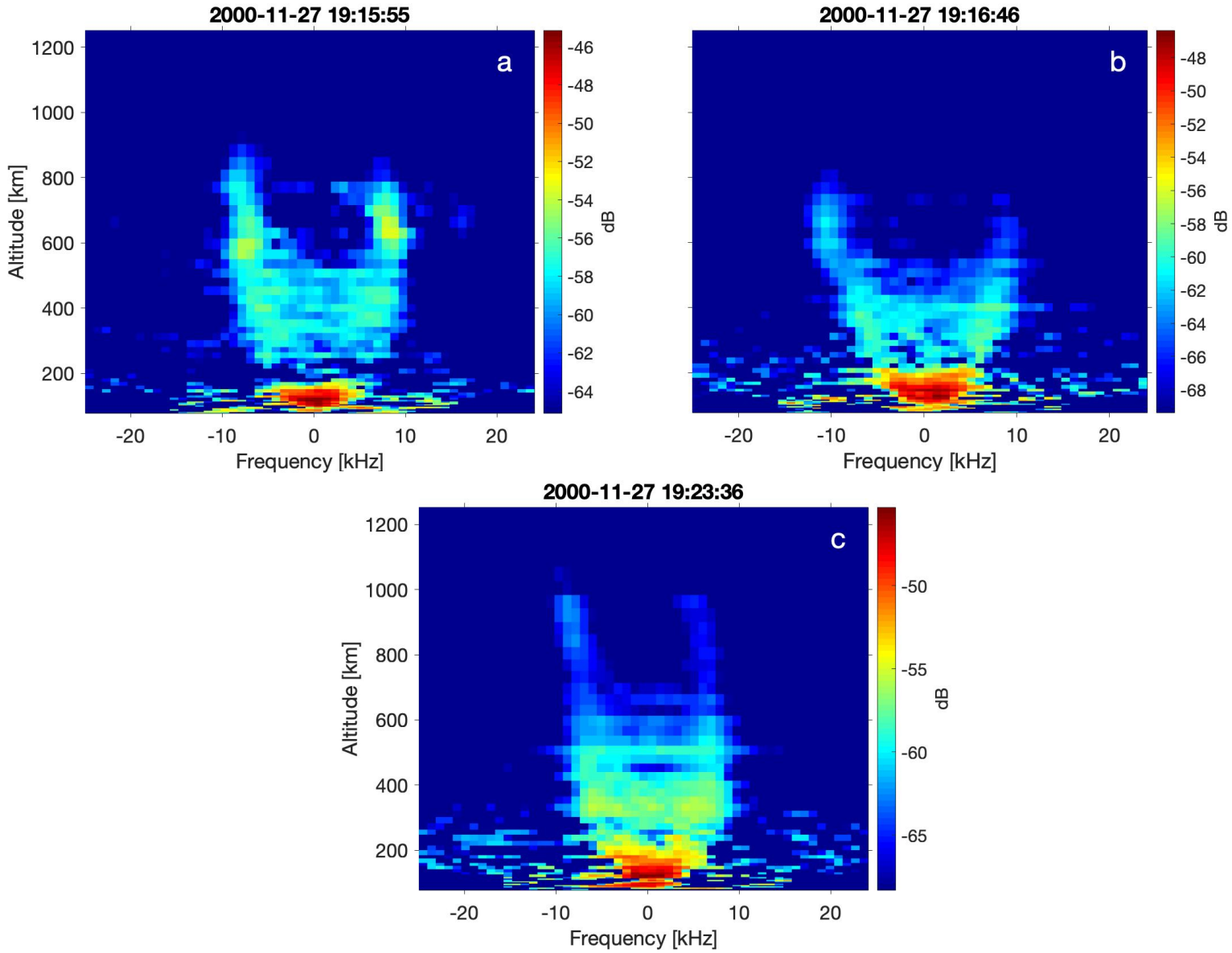

Figure 4.16: The NEIAL events on the evening of 2000 – 11 – 27. a) shows enhancements in both shoulders. b)shows an enhancement in the left shoulder. c) shows an enhancement in the left shoulder and weakly in the right shoulder.

Figure 4.16a shows enhancements in both shoulders. The left shoulder is enhanced at 550 km and the right shoulder is enhanced at 600 km. The intensity for the 630.0 nm line was between 4.2 kR and 4.1 kR. For the 557.7 nm line it was between 3.6 kR and 2.6 kR, the 844.6 nm line the intensity was between 2.2 kR and 2.1 kR. For the 427.8 nm line the intensity was between 407 R and 484 R. The intensities were found from Figure 4.15.

There is a weak enhancement in the left shoulder from 500 km to around 750 km (Figure 4.16b). From Figure 4.15, the intensities of the emission lines were found. The intensity for the 630.0 nm line was 6.1 kR, the 557.7 nm line was 4.0 kR, the 844.6 nm line was 3.2 kR and the 427.8 nm line was 506 R.

In Figure 4.16c we see an enhancement in the left shoulder with an altitude range between 500 km and 1000 km. The right shoulder is weakly enhanced within the same altitude range. Again, the intensities of the emission lines were found from Figure 4.15. The intensity for the 630.0 nm line was between 16.8 kR and 14.9 kR. For the 557.7 nm line it was between 16.3 kR and 12.7 kR, the 844.6 nm line was between 8.4 kR and 7.5 kR. For the 427.8 nm line the intensity was between 1.9 kR and 1.1 kR.

/5 Discussion

In our NEIAL data, we found that 61 of them had the left shoulder enhanced at an altitude above 450 km. The right shoulder was enhanced 36 times over the same altitude range. This agrees with Rietveld et al. [1991] where they stated that the left shoulder was more enhanced compared to the right one at higher altitudes.

All the NEIAL data we investigated in this thesis have a structure where the right shoulder is enhanced at a lower altitude than the left shoulder. The highest altitude for the start of the right shoulder was 750 km, however, most of the time it started about 500 km or below. The only exception is for 19.15.55 UT at 2000 – 11 – 27 shown in Figure 4.16b, where the enhancement of the left shoulder is at 600 km, and the right shoulder is enhanced at 750 km.

There are three NEIAL events that change enhancement in the shoulders during two consecutive data dumps. These episodes happened on 2000 – 11 – 27 and 2003–12–20. They all have enhancements in both shoulders, but one shoulder is more enhanced than the other. All these episodes start with a situation where the right shoulder is more enhanced followed by the next data dump where the left shoulder is more enhanced. The right shoulder enhancement starts at a lower altitude than the left shoulder enhancement. Maximum starting altitude of the right shoulder is 650 km and the minimum of the left shoulder is 550 km. The right shoulder enhancement in the last data dump starts at a lower altitude than the previous dump. For example, in Figure 4.3b and Figure 4.3c from 2003 – 12 – 20, the first data dumps show an enhancement in the right

shoulder from 500 km and in the following data dump it is at 450 km. The enhancement is as low as -55 dB and has a maximum at −44 dB. There was no enhancement in the left shoulder when the power intensity was below −50 dB.

Comparing the geomagnetic activities on these days, we discovered that 2000 − 11 − 27 was a storm day and had small disturbances in the magnetic field (Figure 4.11). For 2003 − 12 − 20, there was no indication by the indices that there was a storm or substorm on that particular day. The magnetometer measured a disturbance of 150 nT around 11.00 UT shown in Figure 4.1, but this is not as severe as the disturbances Rietveld et al. [1991] stated were associated with NEIAL events.

For 2000 − 11 − 27 and 2003 − 12 − 20 there were three consecutive data dumps. The intensity of the 630.0 nm line was always above 10 kR, and the 844.6 nm line was above 1 kR. The intensities of the 427.8 nm and the 557.7 nm lines were close to 0 R. This agrees with Collis et al. [1991], where the 630.0 emission line must exceed 10 kR in intensity in order for NEIAL events to occur. For all these episodes, the 844.6 nm line had a larger intensity than the 557.7 nm line. This agrees with Lunde et al. [2009], where they stated that the 844.6 nm line correlates better with NEIAL events than the 630.0 nm emission line.

The shifting of the enhancements in the shoulders has been shown to be on the order of milliseconds [Grydeland, 2003]. Consecutive dumps of NEIAL episodes is probably related to the duration of the particles precipitation event.

For the NEIAL events at 2003 − 12 − 20, the enhancements were low compared to the average power for all days which was −50 dB. The maximum power was −53 dB. The 630.0 nm line was the emission line with the highest intensity. The 630 nm line was above 10 kR for the most part except at 13.40.23 UT where it was 7.1 kR. The 844.6 nm line was always higher in intensities than the 557.7 nm line even at 13.40.23 UT where they are almost equal. For this day, the power was −54 dB, and the enhancement started at a lower altitude than for the other events that day.

The minimum intensity for the 844.6 nm line is 695 R, and the maximum for the 557.7 nm line is 595 R. Except for this, there is a difference of minimum 400 R between the two lines. At 09.29.49 UT, there is a peak in the intensities of both the 630.0 nm and the 844.6 nm lines. At 13.40.23 UT, there is a peak in the intensity of the 630.0 nm line. However, at 11.04.00 UT and 11.04.07 UT, there is only a peak in the 557.7 nm line. The power of all these events is below average.

All NEIALs in Figure 4.3 have a well defined structure, and the left shoulder is enhanced more than the right one. The left shoulder enhancement is not very stretched in altitude, except at 11.04.07 UT where the left shoulder is enhanced to around 1200 km. The enhancement is not symmetric around the center frequency which indicates ion upflow.

For the events at $2004-01-22$, the 630.0 nm line is more than 10 kR as Collis et al. [1991] stated that it should be. The 557.7 nm line has a greater intensity than the 844.6 nm line. The only exception is for 09.11.27 UT where the intensities are almost equal. The maximum intensity separating them is 1.0 kR. The difference is not very high compared to other events.

All emission lines have a peak at 08.55.02 UT and 09.11.27 UT. The 557.7 nm line and the 844.6 nm line are the only emission lines that have peaks at 09.08.03 UT and 09.14.14 UT. All these times the NEIALs have a good structure and are pronounced except at 08.55.02 UT where they were limited in altitude.

At 09.11.27 where the 557.7 nm and 844.6 nm lines are almost equal in intensities, the 557.7 nm line has a higher intensity, but there is only 88 R separating them. The power is below average for all days investigated, with -58 dB and there is an enhancement in both shoulders.

For the most part, the power of the NEIALs is low with a maximum of -54 dB. The only one with a higher power than average is the event on 08.55.02 UT shown in Figure 4.6a, where the power is -48 dB. The left shoulder is enhanced at a lower altitude than the other episodes of this day. The intensities for all the emission lines are at maximum compared to the other times this day.

On $2001-11-16$, the geomagnetic activity was not very high during all the NEIAL events. In all the events, the right shoulder was enhanced in an altitude range from 300 km to 500 km. At 05.25.18 UT, there is also an enhancement in the left shoulder, but this is weaker than the enhancement in the right shoulder. None of these have an excellent structure or long altitude range.

At around 05.00 UT, there is a negative disturbance in the H component of the magnetic field. The disturbances have a magnitude of 200 nT. This does not agree with Rietveld et al. [1991] where NEIALs are associated with severe geomagnetic disturbances around 500 nT.

Lunde et al. [2007] reported that the 844.6 nm line was a better indicator of NEIAL events than the 630.0 nm line. The reason was that the 844.6 nm line is a prompt emission where as the lifetime of the 630.0 nm line is 110 s. We

investigated our data and found from Figure 4.10a at 03.05.08 UT that there are no peaks in the emission lines. In Figure 4.10b at 05.25.18 UT there were peaks in the 630.0 nm and the 557.7 nm lines. In Figure 4.10c at 05.59.25 UT there was a peak in almost all the lines except for the 630.0 nm line. It is not clear that the 844.6 nm line is a better indicator of NEIALs from our investigation.

The intensities of the emission lines for the events on this day was not high at all. The maximum intensity for the 630.0 nm line was 1.5 kR. The 557.7 nm line or the 844.6 nm line intensities were above the 630.0 nm line intensities for all the times NEIAL events occurred. Often the 557.7 nm line was above the 630.0 nm line, except for 05.59.35 UT shown in Figure 4.10c, where the 844.6 nm line intensities are above the 557.7 nm and the 630.0 nm lines intensities. However, comparing the power in this figure, this time has a weaker enhancement with only −62 dB in contrast to 05.25.18 UT where the power was −48 dB.

Collis et al. [1991] reported that NEIALs are associated with intense red aurora with 10 kR intensity. As seen in Figure 4.10c, the maximum intensity of that line is 1.5 kR which does not support the conclusion of Collis et al. [1991]. We see in Figure 4.8 and Figure 4.10a and b that at lower altitudes (<400 km) the right shoulder is enhanced and the 557.7 nm line intensity dominates. However, an exception at 05.59.25 UT, where the 844.6 nm line has the highest intensity, but the power of the enhancement was weak.

Because the 557.7 nm line is associated with a higher energy of the precipitating the particles than both the 844.6 nm and the 630.0 nm lines, the Parametric decay of Langmuir waves theory may not be the prevailing theory at low altitudes. This theory requires soft particle precipitation. At these lower altitudes, the current driven instability may prevail where it is dependent on an intense local current.

On 2000 − 11 − 27, the NEIAL events in consecutive data dumps have peaks of the 630.0 nm emission line. However, there is also a peak in the 844.6 nm line at 09.24.35 UT and 09.24.48 UT. This day had the highest intensity of the 630.0 nm line of all dates investigated in this thesis. The 844.6 nm line has a higher intensity than the 557.7 nm line with the only exception at 05.26.56 UT where the 557.7 nm line intensity is equal to 844.6 nm line intensity. The minimum intensity for the 844.6 nm line and the 557.7 nm line is 1.1 kR for both lines. The difference between those lines is small with a maximum of 1.5 kR. When the 844.6 nm line is equal to 557.7 nm line, the enhancement is very high in both ion lines. However, for this time the power for the left shoulder is maximum −52 dB, and for the right shoulder it is −58 dB. This is not high compared to the other times this day where the minimum power was −50 dB.

For the NEIAL event at 10.15.34 UT, there is a substantial enhancement in the right shoulder as mentioned. This is the most potent enhancement of all our events, and the left shoulder is enhanced with a power of −49 dB as it also is at 10.15.47 UT. It looks like that the left shoulder is enhanced through the whole data dump, and that the right shoulder enhancement is fading.

At 05.26.56 UT, there were no peaks in the intensity. At 09.24.35 UT and 09.24.48 UT, there were peaks in the 630.0 nm line, the 427.8 nm line and the 844.6 nm line. At 10.15.34 UT and 10.15.47 UT, there was a peak in the 630.0 nm line. It is not in agreement with the results from Lunde et al. [2009] were the 844.6 nm line was found to be a better indicator for NEIAL events than the red line.

On this day, the power of the enhancements is high for almost all the events and the 630.0 nm line is above 20 kR. The same situation can be seen in Figure 4.6a where the power enhancement is high and the 630.0 nm line is above 20 kR. It agrees with the minimum limit of 10 kR for the 630.0 nm line to have NEIALs. It is associated with soft electron precipitation [Collis et al., 1991].

For the NEIAL events on $2000-11-27$, the left shoulder enhancement starts at 500 km. Figure 4.16a shows enhancement in both shoulders, where the right shoulder enhancement is at a higher altitude than left shoulder enhancement. During most of the time the intensity of 630.0 nm line is low with an intensity below 5 kR. It disagrees with Collis et al. [1991]. This statement is mentioned by Lunde et al. [2009] where they researched this particular day.

The time 19.23.36 UT is the only exception from the description above since the intensity of the 630.0 nm line is above 10 kR. However, the intensity of the 557.7 nm line is also above 10 kR. Lunde et al. [2007] investigated the ratio of the 630.0 nm and the 557.7 nm lines intensities and found that NEIALs happens when the ratio is above 5. Our ratio for this day is less than 5. The power was −63 dB. Compared to the other events that day where the power was −53 dB and −60 dB, the power at 19.23.36 UT was much weaker than the other times that day. For all these events there is no pronounced structure of the NEIAL events or very high intensities.

Overall for this evening, the 557.7 nm line has a larger intensity than the 844.6 nm line. There is a peak in all the emission lines before the events happen for all the episodes. The only time where it actually is a peak at the same time as the episode is for 19.16.46 UT. This happens only for the 427.8 nm line and the 844.6 nm line. This is an agreement to Lunde et al. [2009], where they state that the peaks of the intensity of the 844.6 are associated with NEIALs.

There were two events where the 630.0 nm line is below 10 kR and the intensities of 557.7 nm line and 844.6 nm line are almost equal. During this episode, there was a weak power intensity of the enhancement, and for this event, the left shoulder is enhanced.

There is a clear connection between the intensity of the 630.0 nm line and the power of the enhancement. From the figures and investigation we can see that for high power of the enhancement, the 630.0 nm line is above 20 kR.

Because of the theory of the ion-ion two-stream instability may be applicable at higher altitudes and our experiment is at a maximum of 1200 km, it is not possible to check the validity of this theory. There is one incident at 2000 – 11 – 27 where the enhancement is reaching above 1200 km. At these altitudes we may have a relative velocity between O^+ and H^+, but that investigation is beyond the scope of this thesis.

6

Conclusion

This thesis has focused on the relations between the auroral emission lines and NEIALs.

In the previous literature, NEIALs have been associated with a high intensity of the 630.0 nm line with at least an intensity 10 kR [Collis et al., 1991]. Lunde et al. [2007] argued that there needs to be a ratio of 5 of the intensities of 630.0 nm line and 557.7 nm line. In our study, we contradicted both of these associations. There are seven episodes where the intensity of the red line is below 10 kR and six episodes where the ratio is way below 5. During three of these episodes, the red line intensity was below the intensities of the 557.7 nm line or the 844.6 nm line.

Rietveld et al. [1991] argued that NEIAL events are associated with a high geomagnetic activity of 500 nT or more. We have found two days with NEIAL events where the disturbances in the H component of the magnetic field is way below 500 nT. Therefore, severe geomagnetic activity is not always associated with NEIAL events.

The starting altitude for the right shoulder enhancement was typically lower than the starting altitude of the left one. We also found that the 557.7 nm line intensities were larger than the 630.0 nm line intensities at low altitudes (<400 km). Because the 557.7 nm line needs more energy to be emitted and that it is associated with an energy range between 1 keV and 15 keV, then the parametric decay of the Langmuir waves theory is probably not the prevailing

theory at lower altitudes. The typical energy that is associated with this theory is 500 eV. Therefore we suggest that the current driven theory is a better way to describe NEIALs at lower altitudes.

Lunde et al. [2009] stated that the 844.6 nm line had a better correlation with the NEIAL events than the 630.0 nm line. We could not confirm this with our study. The 844.6 nm line did not have peaks for all the episodes. Also, sometimes none of these emissions lines had peaks at all.

There is a possible connection with the red line intensity and power enhancement. For high red line intensities (above 20 kR) we observed a high power enhancement.

At higher altitudes, the red line intensity was always the dominating line which is in agreement with the parametric decay theory.

Future Work

To study the NEIALs and their association with auroral emission lines it would be useful to have a better temporal time and space resolution of the EISCAT data. This would be obtained by the planned EISCAT 3*D* Radar System. It would also be an advantage to use satellite instruments like MEPED to calculate and estimate the energy of the particle precipitation.

Bibliography

Noralv Bjørnå. Agf-304 radar diagnostics of space physics. The Auroral Observatory, Faculty of Science and Technology, Department of Physics and Techonology, University of Tromsø, 2005. FYS-3002, Lecture note delivered 2017.01.25.

Asgeir Brekke. *Physics of the upper polar atmosphere*. Springer Science & Business Media, 2012.

SC Buchert, AP van Eyken, T Ogawa, and S Watanabe. Naturally enhanced ion-acoustic lines seen with the eiscat svalbard radar. *Advances in Space Research*, 23(10):1699–1704, 1999.

H.C Carlson Jr. and A Egeland. The aurora and the auroral ionosphere. In Margareth G Kivelson and Christopher T Russel, editors, *Introduction to Space Physics*, chapter 14, pages 459–500. Cambridge university press, 1995.

Alexander Chernyshov. Ionosphere, ionospheric irregularities. Space Research Institute of the Russian Academy of Science, 2019. ASTRA 2019, Lecture note delivered 2019.03.12.

PN Collis, L Häggström, K Kaila, and MT Rietveld. Eiscat radar observations of enhanced incoherent scatter spectra; their relation to red aurora and field-aligned currents. *Geophysical research letters*, 18(6):1031–1034, 1991.

FRE Forme. A new interpretation on the origin of enhanced ion acoustic fluctuations in the upper ionosphere. *Geophysical research letters*, 20(21): 2347–2350, 1993.

FRE Forme and D Fontaine. Enhanced ion acoustic fluctuations and ion outflows. In *Annales Geophysicae*, volume 17, pages 182–189. Springer, 1999.

JC Foster, C Del Pozo, K Groves, and J-P St Maurice. Radar observations of the onset of current driven instabilities in the topside ionosphere. *Geophysical research letters*, 15(2):160–163, 1988.

Tom Grydeland. *Interferometric and high time-resolution observations of naturally enhanced ion-acoustic echoes at the EISCAT SvalbardRadar : software radar and incoherent scattering*. PhD thesis, University of Tromsø, Tromsø, 2003.

Tor Hagfors. The scattering of e.m waves from density fluctuations in a plasma. In Asgeir Brekke, editor, *Radar Probing of the Auroral Plasma*, chapter 1, pages 15–28. Universitetsforlaget, 1975.

David Harvey. Absorbance and emission spectroscopy. `https://community.asdlib.org/imageandvideoexchangeforum/2013/07/26/absorbance-and-emission-spectroscopy/`, 2013. Acess on 2019-05-18.

Michael C Kelley. *The earth's ionosphere : plasma physics and electrodynamics*, volume 43 of *International geophysics series*. Academic Press, San Diego, 1989. ISBN 0124040128.

Dag Lorentzen. Meridian-scanning photometer (msp). `http://kho.unis.no/msp.htm`, 2002. Acess on 2019-04-03.

Dag Arne Lorentzen. *Vinterhimmelens lysorgel over Svalbard : en faktabok om nordlys*. Nordlyssenteret, AndÃžy, 2007. ISBN 9788299767507.

J. Lunde, B. Gustavsson, U.P. Løvhaug, D.A. Lorentzen, and Y. Ogawa. Particle precipitations during neial events: Simultaneous ground based observations at svalbard. *Annales Geophysicae*, 25(6):1323–1336, 2007. ISSN 09927689.

June Lunde. *Particle precipitation : effects on selected ionospheric phenomena*. PhD thesis, University of Tromsø, 2009.

June Lunde, Unni Pia Løvhaug, and Björn Johan Gustavsson. Particle precipitation during neial events : simultaneous ground based nighttime observations at svalbard. *Annales Geophysicae*, 27(5), 2009. ISSN 0992-7689.

Torsten Neubert and Freddy Christiansen. Small-scale, field-aligned currents at the top-side ionosphere. *Geophysical research letters*, 30(19), 2003.

A Omholt. Particle precipitation: Ionization and excitation. In *Cosmical Geophysics*, page 221, 1973.

Judith Palacios, Antonio Guerrero, Consuelo Cid, Elena Saiz, and Yolanda Cerrato. Defining scale thresholds for geomagnetic storms through statistics. *Natural Hazards and Earth System Sciences Discussions*, pages 1–19, 2017. ISSN Natural Hazards and Earth System Sciences Discussions.

Gerd W Prölss. *Physics of the Earth's space environment : an introduction*. Springer, Berlin, 2004.

MT Rietveld, PN Collis, and J-P St-Maurice. Naturally enhanced ion acoustic waves in the auroral ionosphere observed with the eiscat 933-mhz radar. *Journal of Geophysical Research: Space Physics*, 96(A11):19291–19305, 1991.

H. Rishbeth and O. K. Garriott. *Introduction to ionospheric physics*. : Academic Press; Revised 2000 and Thumb Indexed ed. edition (January 15, 1969), 1969.

MN Rosenbluth and N Rostoker. Scattering of electromagnetic waves by a nonequilibrium plasma. *The Physics of Fluids*, 5(7):776–788, 1962.

Robert Schunk and Andrew Nagy. *Ionospheres: Physics, Plasma Physics, and Chemistry*. Cambridge Atmospheric and Space Science Series. Cambridge University Press, 2 edition, 2009. doi: 10.1017/CBO9780511635342.

Francis Sedgemore-Schulthess and Jean-Pierre St Maurice. Naturally enhanced ion-acoustic spectra and their interpretation. *Surveys in Geophysics*, 22(1): 55–92, 2001.

F. Sigernes, D.A Lorentzen, N. Lloyd, R. Neuber, Degenstein D. Hoppe, U.-P., N. Shumilov, J. Moen, Y. Gjessing, Skartveit A. Havnes, O., E. Raustein, J.B. Ørbæk, and C.S. Deehr. The mysterious red sky on 6 december 2002. `http://fred.unis.no/6dec2002/msp.htm`, 2002. Access on 28.11.18.

A Strømme, V Belyey, T Grydeland, C La Hoz, UP Løvhaug, and B Isham. Evidence of naturally occurring wave-wave interactions in the polar ionosphere and its relation to naturally enhanced ion acoustic lines. *Geophysical research letters*, 32(5), 2005.

M.P. Sulzer. Radar | incoherent scatter radar. In James R. Holton, editor, *Encyclopedia of Atmospheric Sciences*, pages 1812 – 1819. Academic Press, Oxford, 2003. ISBN 978-0-12-227090-1. doi: https://doi.org/10.1016/B0-12-227090-8/00330-4. URL `http://www.sciencedirect.com/science/article/pii/B0122270908003304`.

Anders Tjulin. Eiscat experiments. `https://www.eiscat.se/wp-content/uploads/2016/05/Experiments.pdf`, 2015. Access on 2019-03-11.

J-E Wahlund, FRE Forme, HJ Opgenoorth, MAL Persson, EV Mishin, and AS Volokitin. Scattering of electromagnetic waves from a plasma: Enhanced ion acoustic fluctuations due to ion-ion two-stream instabilities. *Geophysical*

research letters, 19(19):1919–1922, 1992.

G Wannberg, I Wolf, L-G Vanhainen, K Koskenniemi, J Röttger, M Postila, J Markkanen, R Jacobsen, A Stenberg, R Larsen, et al. The eiscat svalbard radar: A case study in modern incoherent scatter radar system design. *Radio Science*, 32(6):2283–2307, 1997.